HHS Public Access

Author manuscript

J Cogn Neurosci. Author manuscript; available in PMC 2017 March 01.

Published in final edited form as:

J Cogn Neurosci. 2016 March ; 28(3): 379–401. doi:10.1162/jocn_a_00903.

Modulation of Frontoparietal Neurovascular Dynamics in Working Memory

Allen Ardestani[1,2], **Wei Shen**[1], **Felix Darvas**[3], **Arthur W. Toga**[1], and **Joaquin M. Fuster**[1]

[1]University of California, Los Angeles

[2]Cedars Sinai Medical Center, Los Angeles, CA

[3]University of Washington

Abstract

Our perception of the world is represented in widespread, overlapping, and interactive neuronal networks of the cerebral cortex. A majority of physiological studies on the subject have focused on oscillatory synchrony as the binding mechanism for representation and transmission of neural information. Little is known, however, about the stability of that synchrony during prolonged cognitive operations that span more than just a few seconds. The present research, in primates, investigated the dynamic patterns of oscillatory synchrony by two complementary recording methods, surface field potentials (SFPs) and near-infrared spectroscopy (NIRS). The signals were first recorded during the resting state to examine intrinsic functional connectivity. The temporal modulation of coactivation was then examined on both signals during performance of working memory (WM) tasks with long delays (memory retention epochs). In both signals, the peristimulus period exhibited characteristic features in frontal and parietal regions. Examination of SFP signals over delays lasting tens of seconds, however, revealed alternations of synchronization and desynchronization. These alternations occurred within the same frequency bands observed in the peristimulus epoch, without a specific correspondence between any definite cognitive process (e.g., WM) and synchrony within a given frequency band. What emerged instead was a correlation between the degree of SFP signal fragmentation (in time, frequency, and brain space) and the complexity and efficiency of the task being performed. In other words, the incidence and extent of SFP transitions between synchronization and desynchronization—rather than the absolute degree of synchrony—augmented in correct task performance compared with incorrect performance or in a control task without WM demand. An opposite relationship was found in NIRS: increasing task complexity induced more uniform, rather than fragmented, NIRS coactivations. These findings indicate that the particular features of neural oscillations cannot be linearly mapped to cognitive functions. Rather, information and the cognitive operations performed on it are primarily reflected in their modulations over time. The increased complexity and fragmentation of electrical frequencies in WM may reflect the activation of hierarchically diverse cognits (cognitive networks) in that condition. Conversely, the homogeneity in coherence of NIRS responses may reflect the cumulative vascular reactions that accompany that neuroelectrical proliferation of frequencies and the longer time constant of the NIRS signal. These findings are directly relevant to

Reprint requests should be sent to Allen Ardestani, Box 951759, 48-129 BRI, 760 Westwood Plaza, Los Angeles, CA 90095, or via aardesta@ucla.edu.

the mechanisms mediating cognitive processes and to physiologically based interpretations of functional brain imaging.

INTRODUCTION

Oscillatory synchrony is widely accepted as a principal mechanism of neural signaling (Fries, 2005; Buzsáki & Draguhn, 2004). An expansive literature demonstrates both local and interregional synchrony in a wide range of frequencies as a function of cognitive operations, such as working memory (WM; reviewed in Wang, 2010). More recently, similar observations have emerged from neurovascular signals, both at rest and during stimulation (reviewed in Bledowski, Kaiser, & Rahm, 2010). The cumulative evidence supports a cortical system in which during WM neuronal assemblies represent and relay information via transient changes in phase and/or amplitude (Siegel, Donner, & Engel, 2012). Much less is known, however, about the temporal dynamics of that cortical system. Although various cognitive processes have been ascribed to particular frequency signatures during brief stimuli, the attribution of particular cognitive operations (e.g., WM) to specific frequency bands is likely to falter when examined over longer time periods separating mutually contingent behavioral events. The main problem is the confounding of variables that change with time and are difficult to disambiguate in those periods: primarily, the activation of overlapping representational networks recruited simultaneously or in succession and the temporal deployment of cognitive integrative functions (WM and executive set, among others) operating on them (Fuster & Bressler, 2015).

It remains debated whether these widely observed neural oscillations are in fact “fundamental” to cognition (encoding the content of WM per se) versus “epiphenomenal” (reflecting the cumulative features of the information as well as the executive actions acting upon it; Lowet et al., 2015). In the former view (e.g., Anderson, Serences, Vogel, & Awh, 2014; Honkanen, Rouhinen, Wang, Palva, & Palva, 2014; Roux, Wibral, Mohr, Singer, & Uhlhaas, 2012; Palva, Kulashekhar, Hämäläinen, & Palva, 2011; Sauseng et al., 2009), quanta of information held in WM are directly represented within the amplitude and/or phase of oscillations. More generally, another proposed mechanism relates WM maintenance to the sustained synchronization of particular frequency bands (reviewed in Sreenivasan, Curtis, & D’Esposito, 2014; Curtis & D’Esposito, 2003a, 2003b). A growing number of studies, however, calls into question the direct attribution of neural function to particular oscillatory synchrony (Buzsáki & Schomburg, 2015; Ray & Maunsell, 2015; Sreenivasan et al., 2014; Friston, 1997). Furthermore, several theoretical considerations challenge the assumption that neural synchrony at any particular frequency “encodes” a specific cognitive process or item of information. In the first place, the methodological approaches that have been used to substantiate claims of that kind largely assume the functional homogeneity of the cortical regions explored. Accordingly, they ignore the hierarchical organization of the activated networks spanning those regions. Furthermore, the possible functional significance of task-induced oscillatory desynchronization has largely been overlooked. When addressed, desynchronization has traditionally been simply interpreted as spectral power shifts from lower frequencies (e.g., alpha) to beta–gamma range synchronization (Fries, Reynolds, Rorie, & Desimone, 2001; Klimesch, 1996). More

recent evidence, however, suggests that the dynamic desynchronization of electrical oscillations, in conjunction with a degree of synchronization, describes the signal dynamics that reflect neural interactions in a more parsimonious manner (Bhowmik & Shanahan, 2013; Hanslmayr, Staudigl, & Fellner, 2012).

To sum up, the current literature provides strong evidence for the role of oscillations in the spatial binding of neural assemblies, but not of their temporal binding (Buzsaki, 2010), that is, their integration across time. How do cortical networks, which bind sensory and executive information in their associative structure, utilize that information in cognitive operations? A related question is, how are perceptual networks integrated across time with executive networks in the perception–action (PA) cycle? One first approach to those questions is to validate the presumption that the compounding of activated networks and cognitive processing in those networks is going to add complexity to their signal manifestations; furthermore, that signal complexity is going to increase as a function of task complexity and task performance. Indeed, a number of empirical and theoretical studies support a direct relationship between signal and behavioral complexity (Elton & Gao, 2015; Stokić, Milovanović, Ljubisavljević, Nenadović, & Čukić, 2015; Barttfeld et al., 2014; Hutka, Bidelman, & Moreno, 2013).

But how do we measure complexity of brain signals in the temporal domain? A promising approach to the temporal dynamics of complexity is the study of cortical oscillations and synchrony, across and within cortical regions, in temporally extended cognitive tasks. Especially suitable is the use of WM tasks with long delays (memory periods) and the concomitant application of electrical and functional imaging methods to the cortex. This study in the monkey was designed to combine the complementary advantages and resolution of two different brain signals: electrical surface field potentials (SFPs) and hemodynamic near-infrared spectroscopy (NIRS). By contrast to studies assuming static or bistable neural activation in discrete time periods (see Mitra & Bokil, 2008), the present investigation allows assessment of signal modulation during sustained cognitive processing. The study of complexity in the temporal evolution of signals, however, poses unique computational and statistical problems. Unlike analyses of stimulus epochs spanning hundreds to several thousand milliseconds, the present WM paradigm, which spans tens of seconds, is less discretely constrained for binning in frequency or time. Therefore, we used an entirely data-driven approach without prior categorization of the data in time or frequency (Maris & Oostenveld, 2007) for the statistical assessment of the dynamics of complex signals (cluster-bootstrap). That analysis of joint variables without preassigned constraints is especially appropriate to long WM delays, when multiplexed interactions are expected to occur between activated cognitive networks and multiple cognitive functions succeeding one another. Our subsequent quantification of variance in both time and frequency band—our operational definition of complexity—was likewise performed directly on those joint variables.

The following hypotheses were tested: (i) At rest, the cortex of the nonperforming animal will show discrete oscillatory patterns in both SFPs and NIRS. In accordance with the resting-state literature (reviewed in Raichle, 2015), even in the absence of task performance, an identifiable signal topography will be present within and across regions (frontal and

parietal). (ii) As cognitive demands are imposed by task performance, patterns of activity will undergo temporal modulations with the succession of presumed cognitive processes. Assuming that those processes will recruit networks of varying sparsity, each with its own unique oscillatory properties, and further assuming that extended task periods will allow for the temporal resolution of those processes, the cumulative effect will be that of a temporal fragmentation of the oscillations that have been present at the peristimulus (memorandum) interval. (iii) The degree of that temporal fragmentation, an index of temporal signal complexity, will correlate with the accuracy and complexity of task performance.

All three hypotheses were confirmed. In general, oscillations underwent dynamic changes in relative synchrony throughout the delay period. The extent and frequency of those transitions varied with the cognitive complexity of behavioral condition (rest, control task, incorrect WM, and correct WM). The nature of that relationship between task complexity and signal fragmentation was reciprocal between electrical and neurovascular signals: Whereas dynamic variability of the SFP signal increased with cognitive demand, that of the NIRS signal decreased. This reciprocity of signal behavior is consistent with the concept that the electrical and hemodynamic signals may be differentially attuned to the degree of specificity of the information they reflect.

METHODS

Subjects and Surgical Preparation

Three rhesus macaques were used as the subjects for this study (subjects G2, C3, and A2). Before introduction into the study, the animals underwent cranial MRI in a 1.5-T scanner with heads fixed in a stereotaxic instrument for precise localization of the planned surgical implants. Two regions of association cortex (Figure 1A), in the hemisphere contralateral to the operant hand for each subject, were defined a priori as the focus of our investigation. One was a region of the posterior parietal cortex (PPC) at the junction of the intraparietal, lateral, and superior temporal sulci, comprising large portions of cytoarchitectonic areas 5 and 7 and implicated in spatial attention and WM (Pesaran, Pezaris, Sahani, Mitra, & Andersen, 2002; Colby & Goldberg, 1999; LaBar, Gitelman, Parrish, & Mesulam, 1999; Courtney, Ungerleider, Keil, & Haxby, 1996; Mesulam, 1981; Heilman, Pandya, & Geschwind, 1970; Critchley, 1953). The other was a region of the lateral pFC straddling the principal sulcus, comprising portions of areas 8, 9, and 46. These prefrontal areas are implicated in WM of at least three sensory modalities: visual (Funahashi, Bruce, & Goldman-Rakic, 1989; Bauer & Fuster, 1976; Fuster, 1973), auditory (Fuster, Bodner, & Kroger, 2000; Braver et al., 1997; Vaadia, Benson, Hienz, & Goldstein, 1986), and somatosensory (Kostopoulos, Albanese, & Petrides, 2007; Ricciardi et al., 2006; Romo, Brody, Hernández, & Lemus, 1999; Shindy, Posley, & Fuster, 1994). Networks in the two ROIs were considered paradigmatic of perceptual and executive networks engaged in the PA cycle (Fuster, 2008; Zhou, Ardestani, & Fuster, 2007; D'Esposito, Ballard, Zarahn, & Aguirre, 2000) and in the temporally integrative function of WM.

Access to the brain was achieved through stereotaxic local craniotomy, exposing the dura overlying the ROIs. Custom tubular stainless steel pedestals (16.85 mm inner diameter) were positioned over the surgical openings. These hollow cylinders were attached to the skull with

dental cement for subsequent securing of recording probes during data acquisition. They were plugged by snugly fitting metal inserts when not in use. Threaded sockets were also embedded in the cement to accommodate adjustable swivel brackets used to fix head position during task performance. The surgical procedures were performed under general anesthesia and sterile conditions, in accordance with protocols approved by the University of California, Los Angeles, animal research committee of the Chancellor. After a recovery period of approximately 3 weeks, daily recording sessions were begun.

Resting and WM Task Conditions

Before surgery, the subjects were acclimated to the laboratory and experimental environment. All experiments were conducted in a dark, sound-attenuated room with the animal seated facing a stimulus–response panel consisting of a horizontal array of three touch-responsive display buttons. The subjects were trained to remain motionless with a hand placed on a pedestal except when prompted to make manual selections. Any superfluous movement above a predetermined threshold would immediately abort a data collection trial. Successful performance was reinforced with the delivery of liquid reward into the animal's mouth. All experimental stimuli, trial timing, and behavioral events (movement, pupil position, foveation time, hand position, performance) were monitored electronically.

Neural activity in the resting state—without extraneous auditory or visual stimuli—was recorded from task-naive animals during 20–240 sec epochs of resting wakefulness with the subject sitting idle. Intervals during which the animal appeared drowsy were excluded from subsequent analysis.

After 28 resting state sessions during which all predefined recording positions (see below) were sampled, the subjects underwent training in the behavioral tasks. Visual stimuli for the behavioral tasks were presented via illumination of the touch-response buttons in different colors, and the subjects' manual selections were registered by photocells adjacent to these buttons. With the subject seated motionless in front of the panel, three different types of visual task were performed (Figure 1B). The first was a control task that had the same operational rules as the WM tasks, described below, with the key difference that the subject's choice had no behavioral dependency on the trial-initiating cue. Control task trials began with the 2-sec illumination of the central disk, white, red, or green. After a 20-sec delay, the animal manually selected a blue light that was always presented in the central position. Trials were allowed to proceed to completion only if the animal foveated the trial-initiating stimulus, as determined by an infrared eye-tracking system (ISCAN). Signals were recorded during performance of the control task as they were in the resting state.

After completion of data collection in the control condition, the animals began training to perform the two visual WM tasks, one with a spatial memorandum (spatial task) and the other with a nonspatial memorandum (nonspatial task; Figure 1B). A trial in the spatial task began with the memorandum, the white illumination of one lateral disk (2 sec). After a 20-sec delay, both lateral disks were illuminated white, and the monkey would select the position of the trial-initiating cue. In the nonspatial task, the monkey had to retain the color of the sample. In this task, the central disk was lit either red or green (2 sec). Following a 20-

sec delay, the monkey would indicate the original color by choosing it from one of the two simultaneously illuminated lateral disks, one red and the other green. Trials were separated by an intertrial interval of approximately 60 sec, and the order of task block presentation (spatial vs. nonspatial) was counterbalanced between sessions. In all task conditions, trials were time-locked to stimulus foveation and would be aborted in the event of excessive movement, premature removal of the subject's hand from the pedestal, or failure to foveate (300 msec minimum) the initial stimulus for each trial. Subjects were considered fully trained upon achieving a criterion correct performance level of 75% for three consecutive sessions. Signals were recorded throughout the training process and later analyzed separately for training and for the fully trained task performance.

Signal Acquisition

In all conditions (i.e., resting state, control task, and fully trained WM tasks), four channels each of SFP and NIRS signals were recorded simultaneously per ROI.

Recording Probes—Recording probes with embedded surface electrodes and fiber-optic cables (Figure 1A), configured to maximally coregister the volumes generating the electrophysiological and hemodynamic signals, were designed to tightly fit each cranial implant. Each plastic cylindrical NIRS/SFP probe contained five fiber optic cables—a central NIRS emitter surrounded by four peripheral detectors or optodes with 5.81 mm interoptode separation. A silver ball SFP electrode interposed between each emitter–detector pair was positioned to maximize overlapping spatial sensitivities between the two recording modalities.

NIRS Recording—Functional NIRS recording takes advantage of the differential light absorption of oxy-(HbO_2) and deoxyhemoglobin (HbR) as endogenous contrast agents through which their concentrations can be calculated (Villringer & Chance, 1997). Reflected light emanating from a central emitter and traversing an arc-shaped volume of cortex was picked up through each of four peripheral and orthogonally oriented solid core (1000 μm diameter) fiber-optic cables. Monte Carlo simulation of photon flux was used to model the optical trajectory taken by light sampled at each detector; that characteristic cortical volume traversed by photons sensed at a particular detector defined a given NIRS channel. The reflected light at each of the detector cables was directed into one of eight spectrophotometers (S-2000, Ocean Optics, Dunedin, FL), where it was spectrally decomposed, projected onto a linear CCD array (1028 elements), and digitized. Sequential full-range raw spectra were stored onto hard disk for offline analyses.

NIRS signals were derived using successive acquisition of reflected light every 35 msec. A continuous wave sampling of broadband optical wavelengths between 790 and 910 nm was used to best discriminate HbO_2 and HbR by their absorption spectra. Concentration changes of both oxy-hemoglobin HbO_2 and HbR (as well as cytochrome C oxidase [Cyt], an intracellular enzyme with absorption properties overlapping those of hemoglobin) were calculated from a modified Beer–Lambert law:

$$\Delta\text{Absorbance} = \left(\varepsilon^{\lambda}_{\text{HbO2}}\Delta\left[\text{HbO2}\right] + \varepsilon^{\lambda}_{\text{HbR}}\Delta\left[\text{HbR}\right] + \varepsilon^{\lambda}_{\text{Cyt}}\Delta\left[\text{Cyt}\right]\right)L^{\lambda}$$

where λ is wavelength, ε is extinction coefficient for the chromophores, and L is optical path length (Villringer & Chance, 1997). Wavelength-dependent path length was computed using a Monte Carlo algorithm (Keijzer, Jacques, Prahl, & Welch, 1989), and extinction coefficients were based on those reported in the literature (Steinbrink et al., 2006; Kohl et al., 2000; Matcher, Elwell, Cooper, Cope, & Delpy, 1995; Wray, Cope, Delpy, Wyatt, & Reynolds, 1988). Other parameters used in the calculation were also in accord with measured values (Steinbrink et al., 2006): anisotropic factor $g = 0.8$; scattering coefficient $\mu_s = 19.1$; local hemoglobin concentration = 0.12 mmol; local oxygen saturation = 80%. A least squares regression was used to solve the above equation across the entire sampled spectral bandwidth (Haaland & Thomas, 1988). Computational models in the literature suggest that such an approach minimizes the degree of spectral cross-talk between chromophores to less than 10% (Obrig & Villringer, 2003; Uludag, Kohl, Steinbrink, Obrig, & Villringer, 2002). The computation was carried out for each successive acquisition (every 35 msec) to produce a time-varying concentration trend for each optical substrate.

The Beer–Lambert analysis yields two concentration profiles for each trial, one for HbO_2 and the other for HbR. The two signals largely mirror each other, with HbR typically having smaller magnitude than HbO_2. Because it cumulatively reflects changes in blood flow, volume, and oxygen content, the computed HbO_2 signal is affected by extraneous factors such as changes in head position, autonomic tone, or variations in hydration state (Obrig & Villringer, 2003). The HbR signal, on the other hand, is less susceptible to such nonneural influences and more directly correlates with the BOLD fMRI signal than does the HbO_2 signal (Steinbrink et al., 2006). Accordingly, in the present data set, the relative prominence of vascular artifacts was greater in the spectral decomposition of the HbO_2 signal than in the HbR signal (Figure 2). The NIRS results described in this study are therefore presented for HbR signals, plotted inversely (with the post-stimulus peak going upward) to match the conventional depiction of BOLD trends. The HbR signal has been illustrated in this fashion elsewhere (Koch, Werner, Steinbrink, Fries, & Obrig, 2009).

SFP Recording—Spatially and temporally coincident with the NIRS signals, monopolar potentials were referenced to the montage ground of all channels, linked to the monkey's contralateral earlobe and to the amplifier ground. Potentials were amplified 500× (Grass Model 15RX; Grass Technologies, Warwick, RI), digitized and filtered between 0.1 and 100 Hz, and stored onto hard disk. A notch filter at 60 Hz was used to attenuate power-line interference. Data were sampled at 1000 Hz and subsequently down-sampled to 200 Hz before analysis. Trials were automatically screened for artifactual SFP activity, set at 3 standard deviations beyond the mean voltage.

Signal Analysis

NIRS Signal Frequency Analysis—Conventional topographic analyses of hemodynamic data generally apply nonparametric signal-processing methods to examine the

temporal course of interactions between time series. Most such methods presuppose relative uniformity of the hemodynamic response function in time and cortical position, although this assumption can falter even within an individual subject (Damoiseaux et al., 2006). Furthermore, repeated BOLD signal amplitudes recorded at even the same position can fluctuate because of gross, state-dependent variations in subcortical neuromodulatory input (Logothetis, 2008). Thus, in addition to assessment of NIRS amplitude, we also tested for the degree of interregional coherence between frontoparietal NIRS signals. The analysis of hemodynamic signals in the frequency domain—particularly slow oscillations at ~0.1 Hz—may provide a more robust characterization of the BOLD signal than conventional time-series assessments (Anderson, 2008; Duff et al., 2008). We therefore utilized a multivariate autoregressive (MVAR) analysis based largely on the methods described by Bressler et al. (Brovelli et al., 2004; Ding, Bressler, Yang, & Liang, 2000), and the MATLAB functions used were adapted from that group's BSMART toolbox (Cui, Xu, Bressler, Ding, & Liang, 2008). Our combination of high temporal resolution NIRS and parametric modeling holds a strong theoretical advantage in assessing hemodynamic oscillatory activity. Because neurovascular dynamics are physiologically constrained to very low frequencies, conventional frequency domain transformations require long data periods to reliably capture their temporal variations. However, because a carefully constructed and verified MVAR model can be assumed to be an accurate predictor of the phenomena underlying the signals, subsequent spectral analyses performed directly on the model have theoretically infinite time resolution (Arnold et al., 1999) and can be applied to relatively shorter time series. Similar MVAR methods have been used successfully in that capacity in studies of autonomic physiology to precisely detect transient compensatory vascular events, at timescales comparable to neurovascular dynamics (Mainardi, 2009).

For the multivariate NIRS analysis of our study, the analysis was restricted to the 0.05–0.15 Hz frequency range to exclude cardiac and respiratory artifacts. To confirm exclusion of nonspecific neurovascular influences or artifacts from the multivariate NIRS analysis, the MVAR analyses were computed also at heart rate frequencies and were verified to not exhibit any trial-related fluctuations in coherence trends.

Electrical Signal Frequency Analysis—Spectral decomposition of the SFP signals into time– frequency representations (TFRs) was performed using a continuous Morlet wavelet transform. The main advantage of using Morlet wavelets is that the kernel width is coupled inversely to its central frequency; time and frequency resolutions are thus determined by setting a fixed number of desired cycles per window. In accordance with previous studies (Kiebel, Tallon-Baudry, & Friston, 2005; Kilner, Bott, & Posada, 2005; Tallon-Baudry, Bertrand, & Fischer, 2001; Tallon-Baudry, Kreiter, & Bertrand, 1999), a wavelet family with a fixed number of seven cycles per window was used. At 20 Hz, for example, this results in a window width of 111.4 msec and a spectral bandwidth of ±2.9 Hz; at 5 Hz, it results in a window width of 445.6 msec and a spectral bandwidth of ±0.7 Hz. Frequencies between 1 and 100 Hz (in 2-Hz increments) were examined with this method.

Each resultant 2-D (time, frequency) color-scale map illustrates the temporal evolution of the frequency domain signal over time, averaged across all individual trials. Prior to statistical analysis, all TFR maps were normalized with respect to their baselines to depict

relative task-induced modulations. The 15-sec period beginning 18 sec before the trial memorandum was used as the baseline. For each trial, the mean and standard deviation of that period were used as standardization factors for each frequency band independently. TFR maps were then smoothed with an adaptive local regression algorithm with sliding window of 500 msec and advancing increment of 100 msec (Mitra & Bokil, 2008).

Synchronization of SFP oscillations between channels was quantified using phase-locking values (PLVs) and plotted similarly. Compared with other computed indices of coherence, the PLV, as described by Lachaux, Rodriguez, Martinerie, and Varela (1999), is less sensitive to signal amplitude and was therefore chosen as the method for quantifying interregional electrical synchrony. The PLV quantifies the intertrial variability of the phase difference between the two time series, within a specified time and frequency range, irrespective of amplitude. This yields a time-varying synchrony factor ranging between 1 (constant phase-lag) and 0 (independent signals) between a pair of signals. PLV maps were baseline-standardized and smoothed in a similar manner as that used for the TFRs

Statistical Analyses—Where noted in figure captions, conventional statistics were used for comparing amplitudes of linear time series. However, those conventional methods were generally not applicable to data sets in this study. First, the assumptions of normality and independence that underlie parametric statistics were not met by several of our data sets. Moreover, the assessment of significance in the multidimensional data sets using traditional statistics was particularly problematic. Brain signals were analyzed across many realizations in time, frequency, trial, and brain position; the specific loci of functional importance, that is, the intersections of those variables, were unknown a priori and had to be determined by inter-rogating large swaths of data. Accounting for chance outcomes arising from multiple comparisons using typical p value corrections was thus not practical. A nonparametric solution to this problem takes advantage of a permutation-based cluster-bootstrapping approach (Maris & Oostenveld, 2007). The method is designed to reduce data dimensionality by objectively combining like-data across adjacent epochs of trial time, frequency, and channel position. Nonparametric statistics are then performed on the clusters using much fewer data points than in the original time series. Significance of so-called clusters can then be assigned using random permutations of values derived from them, without any assumptions on the underlying population distribution. Doing so allows objective dimension–reduction of the data without a priori categorization of the time–frequency maps.

The first step in that analysis approach was to obtain a point-by-point arithmetic difference between baseline-standardized 2-D maps obtained for any two given conditions. The resulting “observed difference map” was then thresholded to include only values that exceeded the 95th percentile of that of mean baseline. Because this step was performed on standardized maps, the qualified data points from this step represented the statistically uncorrected significance level. The specific level of the threshold value has no impact on the overall false-alarm rate of the analysis; as long as it is implemented uniformly, the cluster threshold only affects the desired sensitivity of the analysis. Next, a nearest-neighbor clustering algorithm objectively defined clusters of the thresholded data. The cluster identification procedure did not distinguish between adjacency in the time and frequency

dimensions, making it well suited to address ambiguous functional interdependence of those variables. Once all clusters in the observed difference map were defined by the clustering algorithm, a so-called cluster statistic was assigned to each by summing all the data point values within the cluster. At this point, the observed difference map between two conditions has been segmented into time–frequency clusters—independently for positive and negative values—and each assigned a cluster statistic based on the strength of the difference. A statistical distribution for determining significance was derived from permutations of those clusters randomly drawn from multiple task conditions. Pooling and repartitioning the trials with respect to a particular categorization isolated that variable for interrogation by the analysis. For example, when comparing correct and incorrect trials, all trials from the two conditions were pooled into a single set from which the permutations were drawn. The permutation pool was then randomly divided into two sets, each with the same number of trials as the original. The trials were analyzed and compared just as the observed data had been, an analogous clustered difference map was produced, and the single highest cluster was selected for the permutation distribution. This procedure was repeated 5000 times to produce a null distribution of clusters from the pool of combined correct and incorrect trials, representing the distribution of cluster values that can be obtained when comparing arbitrary pools of trials. Subsequently, each “observed” cluster from the difference map produced by subtracting correct and incorrect trials was compared against the null distribution to compute a p value for each.

TFR findings were assessed for significance using the above approach with MATLAB functions from the Field-Trip toolbox (fieldtrip.fcdonders.nl/). The cluster-boot-strapping analysis was adapted to assess for significant differences between different conditions (i.e., trial vs. baseline, correct vs. incorrect response, spatial vs. non-spatial task, WM vs. control).

Dynamic Variability—A principal hypothesis of this study predicts that the discrete changes in synchrony identified in the immediate peristimulus period will undergo significant modulations when examined over tens of seconds. Quantification of the degree of those modulations is challenging, because no unifying metric exists that encompasses fluid transitions in time and frequency and which can be uniformly applied to signals with vastly different timescales. In light of this challenge, we devised an index of “dynamic variability” that approximates a measure of the complexity of signal transitions within 2-D time–frequency maps. For the interregional SFP phase-locking and NIRS coherence time courses, the standard deviation was computed across all data points contained within a sliding window with a specified time bracket (3 sec for electrical signals and 5 sec for NIRS) and translated in overlapping 1-sec intervals across the entirety of the trial length. The standard deviation for each iteration was plotted across time, producing a graphical representation of the signal variability from the baseline through the task performance epochs. Similar quantification of variability has been applied elsewhere in assessing the stability of fMRI coherence (Rack-Gomer & Liu, 2012). The choice of standard deviation as the measure of variability, as opposed to, for example, a first derivative, was driven by its straight-forward applicability to grouping data points across multiple dimensions (i.e., temporal, spatial, and/or frequency dimensions). It is understood that this analysis will capture both functional and nonfunctional (i.e., noise) contributors to signal variability. However, inasmuch as it will

be applied uniformly to multiple task conditions, any differences observed presumably will reflect underlying differences in neural activation. The significance of differences in dynamic variability between various conditions was computed using a nonparametric Kruskal– Wallis test.

RESULTS

Simultaneous NIRS and SFP signals were collected from both frontal and posterior cortical areas while monkeys performed two visual WM tasks, a control task, and during resting conditions (Table 1).

Oscillatory Resting State Activity

We examined signal dynamics in the resting state to characterize the intrinsic neural background against which task-induced activations occurred. Importantly, the a priori selection of recording positions eliminated the need to delineate ROIs based on statistical thresholding. In both signal modes, the resting state is characterized by sequences of mixed rhythmic activity, best represented in the frequency domain. The NIRS signal in all ROIs exhibits a mean spectral peak at 0.082 Hz (0.072, 0.085, and 0.09 Hz in subjects G2, C3, and A2, respectively), similar to that in previous reports on BOLD fMRI (Vincent et al., 2007). Other local maxima in the NIRS power spectrum appear at frequencies corresponding to the respiratory (mean = 0.32 Hz) and cardiac (mean = 1.89 Hz) rhythms (Figure 2).

To assess hemodynamic signal interactions across cortical regions, we computed correlation values for all combinations of NIRS positions that were sampled simultaneously (Figure 3A). Each “ROI pair” consists of NIRS signals recorded from two positions between cortical sites (interregional pairs), totaling 28 possible combinations. The correlation patterns appear similarly in all subjects and exhibit signal covariance topography that varies with different “seed” regions, in similar manner as described elsewhere in primate BOLD fMRI signals (Yeo et al., 2011; Vincent et al., 2007). Irrespective of the particular topology of the interregional pairings, a distinct distribution of varying signal strengths between regions underscores the presence of intrinsic organized activity observable even in the absence of task performance.

The electrical correlates of those NIRS signals further support the presence of spontaneous functional connectivity in the resting state. Generally overlapping the topography of NIRS interactions, interregional SFP phase-locking activity shows strong phase-locking in the delta (<4 Hz), gamma (30–55 Hz), and—to a lesser degree—high-gamma (65–100 Hz) ranges (Figure 3B). Each of these oscillatory features of resting electrical activity has been described previously in the monkey (Scholvinck, Maier, Ye, Duyn, & Leopold, 2010; Shmuel & Leopold, 2008; Leopold, Murayama, & Logothetis, 2003) or the human (He, Snyder, Zempel, Smyth, & Raichle, 2008; Mantini, Perrucci, Del, Romani, & Corbetta, 2007; Moosmann et al., 2003). However, the present demonstration of their coexistence with concomitant vascular coactivations—without experimental confounds arising from comparing data sets acquired in different subjects—not only reaffirms the neural underpinnings of resting state activations but also illustrates the multidimensional spectral

dynamics occurring within a surface-defined cortical domain. Task-induced modulations of interregional signal interactions are superimposed upon these intrinsic coactivations.

Task-induced Modulations of Oscillatory Activity

We next investigated how intrinsic neural activity, present in the absence of overt external stimulation, undergoes changes during performance of cognitive tasks. For the NIRS and interregional electrical PLV computations, trials were pooled across WM memorandum type (i.e., spatial and nonspatial) because no significant large-scale difference were identified between those conditions.

Intraregional NIRS—Task-induced NIRS signal modulations are seen beginning approximately 3 sec before the onset of the trial-initiating cue. Because the intertrial interval was kept relatively constant throughout recording sessions, signal fluctuations preceding that cue were presumably induced by expectancy of the upcoming stimulus. Prestimulus NIRS activity consists of a relatively protracted deflection, upward or downward, that significantly differs from the preceding baseline period. Likely reflecting a top–down influence that impacts the perception and subsequent utilization of that stimulus (Engel, Fries, & Singer, 2001), that prestimulus NIRS activity on average is significantly attenuated in incorrect trials in comparison with correct WM trials (Figure 4). In the human, analogous prestimulus BOLD coactivations have similarly been correlated with accurate task performance (Sylvester, Shulman, Jack, & Corbetta, 2009).

During the ~500-msec period beginning with stimulus foveation, the NIRS time course on average exhibits a discrete downward deflection that is most pronounced in pFC during performance of control task trials (Figure 4). Reflecting a transient increase in HbR concentration time-locked to a stimulus, we interpret that NIRS response as an “initial dip” resulting from oxygen consumption directly coupled to increased neural activity (Vanzetta & Grinvald, 2008). The initial dip magnitude does not significantly differ between correct and incorrect WM trials or between different WM memoranda (i.e., spatial vs. nonspatial).

The early-delay phase is marked by a NIRS peak occurring at approximately 5 sec after cue onset as well as a smaller ensuing peak at about 10 sec. The relative NIRS amplitude at those epochs is uniformly smaller in the control task than in the WM tasks. The concurrent NIRS signal in PPC, which presumably plays a relatively more sensory-specific WM role (Snyder, Batista, & Andersen, 1997), shows significant memory-dependent differences (i.e., differing between WM and control task trials) but no performance-related changes (i.e., differing between correct and incorrect trials; Figure 4).

Later in the delay interval, approaching the choice stimuli, NIRS signal magnitude generally increases. This late-delay peak in pFC is significantly greater in correct trials than in incorrect trials and the lowest in control task trials (Figure 4). Similar performance-related differentiation at the late-delay peak is seen in PPC, although with less consistency across subjects.

Intraregional SFPs—TFRs were used to depict the time-varying changes in band-power across frequency bands. A clustering permutation approach allowed direct performance of

statistical analysis on these maps, without the need for a priori parcellation of the data into time or frequency bins. Because this clustering algorithm was optimized for detection of broader, temporally protracted trends, it has limited sensitivity for evaluation of transient changes in synchrony or subtle task-dependent changes during the brief cue presentation interval. Nonetheless, in accordance with other primate studies (Buschman, Denovellis, Diogo, Bullock, & Miller, 2012; Siegel, Warden, & Miller, 2009; Womelsdorf & Fries, 2007), electrical activity during the cue presentation epoch in all subjects demonstrates an (at least transient) increase in gamma power, especially in pFC (Figures 5–7). More prominent, and present in both ROIs, is a brief decrease in beta band-power at the cue, also similar to prior reports (Siegel et al., 2009). Concomitant alpha-band activity at the cue epoch shows a predominantly negative change in synchrony. The spectral profile at theta and delta range frequencies is at least partially influenced by the power spectrum of the evoked response and, for the most part, shows a strong increase in peristimulus synchrony.

The beginning of the delay epoch is marked by cessation of the memorandum stimulus. The oscillatory dynamics during this period exhibit some idiosyncratic features across subjects, similar to the variability seen in other WM studies with memory epochs spanning greater than a few seconds (Sarnthein, Petsche, Rappelsberger, Shaw, & von Stein, 1998; Gevins, Smith, McEvoy, & Yu, 1997). However, the most reliable and prominent changes are evident in frequencies greater than 30 Hz. In WM trials performed by subject G2 (Figure 5A, B), band-power in this range gradually increases and peaks in the mid-delay, followed by a steady decrease to sub-baseline levels up to presentation of the choice stimuli. subject C3 (Figure 6A, B) exhibits a similar gradual decrease in high-frequency synchrony over the course of the delay, more pronounced in the spatial WM task. High-frequency power dynamics in subject A2 (Figure 7A, B) follow an inverse pattern, steadily increasing throughout the delay epoch. In all subjects, the absolute magnitude of these synchrony changes is greater in correct trials than in incorrect trials (Figures 5–7A, B, bottom row); that synchrony in the beta–gamma range is also greater in correct WM trials than in control task trials (Figures 5–6C). This high-frequency power trend is, on average, more robust in the spatial WM task than in the nonspatial WM task for subjects G2 and C3 (Figures 5–6D), especially in PPC, similar to task-specific activations reported elsewhere (Buschman et al., 2012).

Dynamics at lower frequencies demonstrate a complementary trend throughout the delay epoch. In all subjects, theta range band-power in pFC steadily increases throughout the delay, in fact switching from sub-baseline to supra-baseline values in subjects C3 and A2. Theta range band-power in PPC notably differs from that of pFC, on average showing decreased relative synchrony toward the end of the delay (Figures 5–7, right columns). Although this trend does not significantly differ between correct and incorrect WM trials (Figures 5–7A, bottom row), it does differ from the relatively static supra-baseline level of theta synchrony seen in control task trials (Figures 5–6C). Alpha range dynamics during correct WM trials in all subjects and positions show an overall relative decrease in synchrony, present in varying duration throughout the delay. The degree of relative desynchronization is decreased in incorrect spatial WM trials in PPC (Figures 5–7B, right columns). Control task trials show an alpha trend opposite to that seen in correct WM trials,

with alpha-band power either persistently increased or steadily rising, rather than progressively decreased throughout the delay (Figures 5–6C).

Interregional NIRS Coherence—To assess variations in cross-cortical network activation, interregional signal interactions were also examined. For NIRS, these interactions were quantified using coherence measurements between all 28 pairs of frontoparietal data signals. For subjects G2 and C3, successful WM task performance induces a uniform increase in interregional coherence which peaks in the early delay (at $t = 4.2$ and 7.8 sec, respectively; Figure 8A, top row). This is followed by a decrease in coherence to sub-baseline levels, which rebounds again in the last several seconds preceding the choice stimuli. Compared with correct WM trials, incorrect trials elicit a similar peak, though occurring 1–2 sec later in the early delay, followed by a blunted nadir in the later delay (Figure 8A, middle row). In control task trials, that signal pattern appears further attenuated and less uniform across ROI pairs (Figure 8A, bottom row).

Distinct from the actual magnitude of interregional coherence across different task epochs, we next examined the temporal and spatial homogeneity of the coherence trends across different ROI pairs. To that end, we computed time courses for the fluctuations in the variability of the coherence measurement throughout the trial. In both subjects G2 and C3, coherence modulations induced by correct WM task performance exhibit relatively little change in their variance (Figure 8B). In other words, although coherence values do rise and fall, they do so gradually and uniformly across ROI pairs in correct trials. In contrast, in incorrect WM trials, interregional NIRS coherence exhibits more variability during the delay period, and in control task trials, it does so to an even greater extent. The effect is maximally seen in subject G2 during the second half of the delay ($p = .01$, Kruskal– Wallis) and in subject C3 during the first half of the delay ($p = .02$, Kruskal–Wallis). No task-dependent differences in variability are present in the baseline epochs of either subject ($p = .25$ and $p = .4$, respectively).

Interregional SFP Phase-locking—The electrical correlates of WM-dependent network activity were examined by comparing interregional phase-locking between different task conditions. PLV changes were plotted in 2-D TFRs and analyzed similarly as for local band-power. At the cue epoch, the most consistent finding is the transiently increased theta range phase-locking (Figure 9, left columns). Although our cluster algorithm was not attuned to detect differences in such a transient epoch, this brief increase in phase-locking appears most prominently in correct WM trials, less so in incorrect WM trials, and least so in control task trials (Figure 9, right columns). At higher frequencies, stimulus-induced PLVs in correct WM trials consistently decrease in the beta range and increase in the gamma range, resembling the dynamics reported elsewhere in the primate (Salazar, Dotson, Bressler, & Gray, 2012; Siegel et al., 2009; Buschman & Miller, 2007; Womelsdorf & Fries, 2007). Phase-locking at those higher frequencies shows some significant task-dependent differences among different subjects (Figure 9, right columns).

In the delay phase, all subjects show robust PLV modulations in the beta and gamma ranges. In subject G2, high-frequency phase-locking after the cue epoch steadily increases through the mid-delay, followed by a decrease to sub-baseline levels in the 6 sec preceding the

choice (Figure 9A, left column). Both the mid-delay peak and late-delay nadir show their highest absolute magnitude in correct WM trials, intermediate magnitude in incorrect WM trials, and lowest magnitude in control task trials (Figure 9A). High-frequency dynamics in subject C3 show a similar task dependence and likewise decline over the course of the delay, though without first reaching a supra-baseline peak in the early delay (Figure 9B). The time course of beta–gamma phase-locking in subject A2 does not appear as prominent as that of the other subjects, though a similar task dependence is evident when comparing correct and incorrect WM trials (Figure 9C).

At lower frequencies, converse delay period PLV fluctuations occur. All subjects exhibit a concomitant increase in delta-range PLV in the late-delay epoch. This in general follows the same task differentiation pattern seen at higher frequencies, that is, strongest in correct WM trials and weakest in control task trials. Alpha range PLV dynamics, on the other hand, follow a more variable pattern. Alpha phase-locking in subject C3, and more prominently in subject G2, increases in the late delay. The alpha-band PLV trend in subject A2 also significantly differs from baseline in the late-delay period, although that trend follows an opposite direction, appearing significantly below baseline levels at that epoch (Figure 9C).

The cumulative phase-locking data show that several frequency bands consistently exhibit trial-induced modulation over time, as well as characteristic patterns of task differentiation. Although some nuances differ between subjects, the phase-locking dynamics uniformly undergo the greatest degree of modulation in correct WM trials, followed by incorrect WM trials and control task trials. To quantify that phenomenon, we applied the same sliding window variability analysis described above for the NIRS coherence data to the interregional SFP phaselocking maps. A Kruskal–Wallis test was applied separately to the baseline (t = −11 to −5 sec), peristimulus (t = −1 to 5 sec), and late-delay (t = 16–22 sec) periods. The time course was divided in this manner to theoretically minimize overlap between the predominant cognitive processes occurring at different trial epochs. In the three subjects, dynamic variability in time and frequency (across the 1- to 100-Hz range) increases at the sample epoch and again in the delay epoch (Figure 10). The degree of that variability consistently appears highest in correct WM trials, less in incorrect WM trials, and least in control task trials. In contrast, the degree of time–frequency variability is constant and uniform in the baseline of all conditions. The subdivision of the variability data into composite frequency bands highlights those frequency ranges whose degree of dynamic variability significantly correlates with task complexity (Table 2). In all subjects, the degree of gamma range modulation varies with task complexity at both the sample and delay epochs. In general, beta range variability shows similar task dependence as gamma in the delay epoch, but not at the sample. Conversely, alpha range variability correlates with task complexity mostly at the sample epoch rather than in the delay. Theta and delta range variability does not consistently correlate with task complexity.

DISCUSSION

To our knowledge, this study is the first to combine electrical recording with functional brain imaging in primates performing memory tasks with prolonged memory retention epochs. The purpose was to examine the temporal dynamics of task-induced neural oscillations and

to demonstrate that their degree of modulation—rather than their magnitudes—most closely reflects the cognitive processes under investigation. At rest, the patterned interregional coactivations seen in both the NIRS and SFP signals point to intrinsic organization of the brain that is measurable in both signal domains. It is upon background oscillations that task performance exerts its spectral impact. The task-dependent signal trends that emerge during the expanded delay epochs presumably reflect several sequential cognitive operations that take place in the course of task performance. In both the NIRS and SFP signals, those trends appear most prominently at the sample and delay epochs and generally differ as a function of task performance, not only in timing but also in magnitude. Although comparable task-related changes are observed across subjects, the particular magnitudes and directions of their underlying dynamics differ, most notably in the electrical domain. Similar variability in electrical oscillations as a function of brain location and cognitive state has been reported in the human (Meltzer et al., 2008). Independent of those particular signal variations, however, the degree of modulation of electrical signals exhibits a consistent gradation as a function of cognitive complexity. That is, the greater the cognitive demands of the task (i.e., control task < incorrect WM < correct WM), the greater the degree to which interregional electrical phase-locking is modulated. These findings accord well with computational models in which delay epochs greater than ten seconds induce temporal decorrelation concurrent with ongoing local synchronizations (Battaglia, Brunel, & Hansel, 2007). Conversely, the NIRS signal shows an opposite relationship, where greater task complexity is associated with relatively weaker modulation of interregional NIRS coherence. This inverse relationship likely stems from the differential sensitivity of these two signal modes to different aspects of neural binding and behavior (Logothetis, 2008). Furthermore, the absolute magnitude of synchrony appears less functionally relevant than its modulation over time, and the two, magnitude and modulation, in fact appear largely independent of each other. For example, at rest the delta and gamma frequency bands exhibit the highest absolute PLVs, whereas task performance induces the highest degree of modulation in the gamma band and the least in the delta band. From those findings, we conclude that the critical binding element is not the absolute magnitude of signal synchrony but rather its modulation in the oscillatory context in which it occurs. This conclusion accords well with previous descriptions of temporally complex and variable modulations of network dynamics underlying cognition (Stokes et al., 2013; Meyers, Qi, & Constantinidis, 2012; Barak, Tsodyks, & Romo, 2010).

These conclusions depart from the relatively simplistic attribution of discrete cognitive contents or operations to frequency-specific encoding. Rather, they conform to a hierarchical construct in which local and large-scale networks are differentially and selectively modulated to jointly serve complex behavior. The cumulative oscillatory interactions induced by a cognitive operation would constitute the “spectral fingerprint” (Siegel et al., 2012) of the network that generates them, rather than a “code” of information. With this theoretical construct in mind, our findings lend support to a network paradigm of cognitive organization characterized by neural assemblies that are widely distributed, hierarchical, and highly overlapping.

Hierarchical and Overlapping Organization of Cognits

On the basis of anatomical, physiological, neuropsychological, and imaging studies, one of us (Fuster, 2009) has postulated large cortical networks (cognits) that not only store memory and knowledge but, when activated, serve other cognitive functions as well—attention, perception, language, and intelligence. Three major characteristics make the cognit model exceptionally plausible: (a) the hierarchical organization of cortical memory; (b) the overlap and interconnectivity between memory networks of different hierarchical level (heterarchy); and (c) the relational nature of the cognitive code, essentially consisting of associations established in cortical networks between features of sensory stimuli and/or motor actions.

The present results support the hierarchical organization of cognits that intervene in WM as postulated by Fuster and Bressler (2012). Our underlying assumption is that each network has a certain “frequency signature,” defined by its relational structure, without implying that that frequency itself contains any specific information in the network. Within each ROI, oscillatory field potentials show differential modulations at different frequencies and variable band-power/ PLV interactions, indicating computational complexity (Freunberger, Fellinger, Sauseng, Gruber, & Klimesch, 2009). These cross-frequency interactions are understandable in a hierarchical paradigm. In general, any evidence of frequency comodulation in the cortex can be considered evidence of network nesting (Canolty & Knight, 2010; Lisman, 2010) and thus, indirectly, of hierarchical cognit organization. Although a comprehensive cross-frequency analysis within and between signal modes is beyond the scope of the present article, our data point to numerous examples of such comodulation between frequencies by demonstrating that the dynamic variability across pooled frequencies correlates with behavioral complexity. By further demonstrating that this correlation persists even when the broadband electrical signal is decomposed into traditional bands, we show that modulation within the same frequency band over time likewise contributes to network organization. The prominence of those spectral interactions varies by cortical location, task, and correctness of behavioral response. Such findings accord well with the concept that oscillatory nesting is modulated by cognitive-driven interactions, as opposed to being strictly biophysical couplings (Jensen, 2006). Summing up, the profuse signal transactions suggested in our data set point to complex dynamics even within a single surface-defined volume of cortex.

Within that organizational model, any signal differentiation with respect to various aspects of task performance presumably reflects the hierarchical level of the networks that intervene in that performance. Across signal modes and both within and between regions, prominent signal differences occur as a function of accuracy of WM performance (correct vs. incorrect trials) and WM dependence (control vs. WM tasks). This suggests that the network dynamics subserving the processes that differentiate those conditions are distributed and operant at that mesoscopic level. In contrast, the absence of signal differentiation as a function of memorandum (i.e., red vs. green, left vs. right) suggests that information with that degree of specificity is represented in networks at a different hierarchical level. As demonstrated elsewhere in the literature (Fuster et al., 2000; Romo et al., 1999; Funahashi et al., 1989), such specific information may be mediated by more local neuronal assemblies, as evinced by local field potentials or unit activity. At an intermediate level, the general

category of information retained in WM (i.e., spatial position or color of the memorandum) yields differential signal features only in intraregional SFPs, implying an intermediate level of representation not manifested in hemodynamic or interregional electrical signals. Encompassing the various hierarchical features of task performance is the cognitive complexity of such performance. That cognitive complexity (increasing from control to correct WM) comprises a combination of accuracy and memory contingency and strongly correlates with cross-cortical signal complexity in both electrical and hemodynamic domains. However, it deserves emphasizing that the different manifestations of complexity in hemodynamic and electrical signals are still compatible with a hierarchical interpretation of the dynamically involved networks.

Thus, in accordance with the hierarchical framework, that reciprocity between electrical and vascular phenomena reveals fundamental differences between the functional architectures suggested by each. Several investigations have demonstrated relatively linear neurovascular coupling induced by concrete sensory stimuli in primary sensory cortex (Raichle & Mintun, 2006; Logothetis, Pauls, Augath, Trinath, & Oeltermann, 2001; Mathiesen, Caesar, & Lauritzen, 2000). However, in the context of higher-order cognition and within association cortex, linear relationships may not apply, and the same may be true for the functional relationships between the functional generators of the two signals. Experimental and theoretical evidence, reviewed by Logothetis (2008), suggests that neurovascular signals in particular reflect modulatory neural influences such as motivation or attention. Those impose global alterations in the dynamic equilibrium between excitation and inhibition, upon which faster, task-specific activations operate. The inverse relationship with respect to task complexity seen here between electrical and NIRS signals is consistent with their functional complementarity. Overall, the direct relationship between interregional electrical complexity and task complexity can be explained by increasingly multiplexed network dynamics fragmenting a uniform oscillatory baseline. In contrast, the inverse relationship between interregional NIRS complexity and task complexity can be explained by the temporally and spatially homogenizing neuromodulation reflected by a slower and more global hemodynamic signal.

Cognit Dynamics in the PA Cycle

The two large cortical areas explored in our experiments lie in the highest structural stages subserving the PA cycle, the cybernetic flow of information processing that links the organism to its environment in goal-directed behavior (Fuster, 2009). Thus, our recorded signals presumably reflect transactions within and between perceptual and executive cognits at the top of that cycle. Because reentry is essential to the operations of the cycle and of WM (Compte, Brunel, Goldman-Rakic, & Wang, 2000), signal periodicity and oscillation are to be expected during WM trials. Reentry and reverberation are in fact inherent traits of cognits even at rest. The structural (connective) organization within and between cognits presumably generates large-scale reverberatory signals giving rise to the slow oscillations observed in the resting state, indicating the presence of hierarchical network activity even in the absence of behavioral activity.

The connective organization at rest constitutes the substrate upon which the cognitive dynamics of the PA cycle take place. In functional terms discussed elsewhere in the literature, the constraints set by large-scale resting state interactions exert a “canonical” top–down influence (Siegel et al., 2012; Engel et al., 2001) upon the cognits successively activated in the PA cycle. The sequential activation of those cognits can explain the signal dynamics that we observe during task performance. Indeed, in WM, cognits representing sensory as well as executive aspects of the task must sustain their activation for relatively long periods of time to temporally bridge the interval between perception and action.

Our data suggest that the successive cognit activations mediating integration in the PA cycle begin already before trial onset. In this respect, it stands to reason that the apparent modulation of certain sectors of the cortical hierarchy in the seconds leading up to the cue would be expected to facilitate the effective mnemonic encoding and retention of the memorandum. That preparatory modulation would serve the attentional set, both perceptual and executive (Fuster & Bressler, 2015), essentially consisting in the priming of cognits. The apparent inter-subject variability in NIRS coherence seen in that epoch immediate preceding the stimulus could possibly arise from the varying predominance of overlapping, though competing, cognits encroaching in the NIRS-sampled loci during attentional set. In the human, similar discrepant responses to task performance may arise from overlapping contributions of intrinsically anticorrelated neural networks, including “dorsal attentional” and “default mode” network systems (Fox et al., 2005). Because the to- pography of those networks varies by subject and largely overlaps (Doucet et al., 2011; Yeo et al., 2011), signals reflecting macroscopic neural activity can be primarily influenced by the activity of one network over the other (Smith et al., 2012). In any event, in accord with our findings, prestimulus BOLD dynamics reflecting ineffective or insufficient network activity has been shown to predict poor task performance in the human (Eichele et al., 2008).

Our use of extended behavioral timescales during WM task performance allowed the assessment of signal dynamics underlying protracted cognitive activity—including mnemonic maintenance, motor preparation, and suppression of extraneous interference—that have inherently long time constants and are supported by frontoparietal networks (Curtis & D’Esposito, 2003a). Of note, impulses elicited by eye movements undoubtedly also contribute to the cumulative signals observed during task performance. However, inasmuch as we do not know of any published evidence of differential eye motion during delay-task performance, nor do we have any hypothetical explanation for it if present, we parsimoniously conclude that the presence of saccadic impulses does not impact our inferences from comparisons of task-specific activations. During and immediately following cue presentation, those dynamics reflect perceptual and mnemonic processes (Quintana & Fuster, 1999). Whereas the ongoing rhythms in the resting state may grossly influence the activation of many cognits, a salient stimulus can transiently disrupt the oscillatory steady state present in them at rest (Friston, 1997) and possibly “initiate” PA cycle activity. We argue that the functionally relevant features of the stimulus can impact the type and extents of cognit activation. In our SFP data set, although that peristimulus activation undoubtedly was also influenced by the frequency spectrum of the evoked-response potential as well as saccadic impulses, these phenomena cannot fully explain the significant gradations in signal variability seen as a function of task complexity. In the NIRS domain, task-dependent signal

amplitude changes could be interpreted as cumulative changes in regional activation. At the cue, a differential WM versus control (but not correct vs. incorrect) deflection in the NIRS initial dip amplitude is consistent with the prefrontal inhibition of the urge to prematurely select the cue stimulus. That impulse would be expected to be stronger in the control task, where the cue and choice visual stimuli are operationally more similar than in WM trials. BOLD signal correlates of a comparable suppression of automatic responses have been described in the human (Curtis & D'Esposito, 2003b; Connolly, Goodale, Menon, & Munoz, 2002); with our high temporal resolution NIRS signal, we detect the same phenomenon in the initial dip. In the electrical domain, where faster and more variable band-limited oscillations are observed, the overall gradations in interregional PLV complexity bear the most direct correlation with performance. The highest degree of SFP complexity appears at the cue epoch of correct trials, in which presumably a more successful or effective mnemonic activation occurs. Possible mechanisms underlying that complexity include a phase reset of ongoing rhythms (Rizzuto et al., 2003) or fragmentation of neuronal clusters (Wang, 2010) in more highly recruited cell assemblies. Accordingly, the concretely sensory cue of the control task, which carries less complex associations imposed by the task rules, results in relatively less SFP complexity. When its frequency components are examined, the differential SFP complexity arises primarily from beta–gamma and alpha bands. This agrees with previous reports of top– down control reflected in high-frequency (Buschman & Miller, 2007; Womelsdorf et al., 2007) as well as in alpha range (Sadaghiani et al., 2012; Freunberger et al., 2009) dynamics. In contrast to these dynamics seen in the electrical signal, interregional NIRS coherence does not exhibit discrete peaks at the stimulus and delay epochs. That finding may arise in part because of the inherently slower time constant of the hemodynamic signal and from differing vascular impulse response functions across subjects with different lags in that hemodynamic response.

Following the peristimulus epoch, the balance between mnemonic, preparatory, and other processes continues to shift, as multiple networks are recruited to varying degrees. Inasmuch as cognitive demands differ according to task, the temporal integration provided by the PA cycle likely plays a less prominent role in the control task than in WM tasks, although it is suboptimally activated in incorrect trials compared with correct ones. Similar to correct–incorrect differentiation seen in BOLD amplitude in humans (Pessoa, Gutierrez, Bandettini, & Ungerleider, 2002), early-delay NIRS activity in pFC significantly differs between correct and incorrect trials. In PPC, which presumably plays a relatively more sensory-specific WM role (Snyder et al., 1997), we see significant control vs. WM, but no correct vs. incorrect, NIRS signal differentiation. Compared with the NIRS signal, SFP dynamics show more variable modulations in relation to the PA cycle. The temporally complex SFP dynamics in WM tasks, primarily in higher frequencies, are absent in the control task. Instead, control task trials exhibit persistent theta–alpha dynamics in the delay epoch, possibly reflecting nonspecific cognit activation across all trials (Asada, Fukuda, Tsunoda, Yamaguchi, & Tonoike, 1999; Ishii et al., 1999). That may be because performance of the control task is relatively automatic, not requiring the higher cortical integration of perceptual and executive functions required by WM tasks. In any event, as in the cue epoch, the most robust task-dependent signal feature during the delay is the modulatory complexity of the interregional SFP phase-locking. Interregional phase-locking steadily increases throughout the delay

period and exhibits a similar direct correlation with task complexity as seen at the cue. Because the operational demands of correct and incorrect WM trials are identical, differing signal complexity between the two may be attributable to differing efficacies of activation of the same cognits or to failure at any step of the PA cycle before incorrect responses. On the other hand, interregional NIRS coherence continues to show an opposite pattern as function of mnemonic contingency and performance accuracy.

Conclusions

Our findings support the notion that over protracted task performance intervals, interactive cognits signal one another via the modulation of preexisting associations. The interactions present in the resting state can bias the probabilistic activation in WM of the many different cognits that are structurally linked in long-term memory and can be engaged in task performance. In the electrical domain, that engagement results in rapid fluctuations in intraregional synchrony and cross-cortical phase-locking. Those fluctuations show nuanced variations across subjects but share a common increase in complexity as a function of cognitive task complexity. That is, oscillatory complexity is highest during correct WM performance, in which the PA cycle is maximally activated, and not so much in other conditions where that activation is either ineffective or unnecessary. This suggests that the information represented by the activated cognits is not encoded by discrete changes in band-limited synchrony but rather reflected in higher-order modulations of the cumulative oscillatory interactions within and between cortical regions. The NIRS signal, on the other hand, is morphologically less differentiated as it reflects wide variations in cognit activity. Accordingly, NIRS amplitude exhibits robust performance-related signal differences uniformly in all subjects. Furthermore, interregional NIRS coherence, in contrast to interregional SFP phase-locking, shows less complexity during cognitively demanding conditions, reflecting a more global neuromodulatory influence on cognits.

Overall, the activation of an ROI cannot be treated with a single quantitative metric as if it were a homogenous volume of tissue. Simple explanations relying on regional electrophysiological synchrony or changes in BOLD signal are insufficient to characterize neural communication in the brain (Logothetis, 2008; Friston, 1997). Rather, using the hierarchical model of the cognit, we propose that the content of the representations and the cognitive operations upon them are inseparable. A theoretical approach to understanding brain function based on such a hierarchy—in cortical space, frequency, and time—could reconcile some discrepant reports in the literature by placing them in a spatiotemporally mesoscopic framework (Freeman, Ahlfors, & Menon, 2009). In any case, the adoption of the cognit paradigm may be one step closer to a more mechanistically realistic interpretation of brain function in cognition. Our theoretical framework could help guide future studies examining cross-frequency interactions and expanding the current methodology to larger and more complex memory networks.

Acknowledgments

The authors thank Bill Bergerson and Bradford Lubell for their technical assistance; Warren Grundfest and Jens Steinbrink for advice on NIRS signal acquisition and analysis; Ivo Dinov, Richard Leahy, Eric Maris, and Partha Mitra for lending their statistical and signal processing expertise; and Steven Bressler and Walter Freeman for their

valuable comments during manuscript preparation. This work was supported by NIH grants R01MH072641 and 9P41EB015922, NASA GSRP grant NNX06AH25H, and Sigma Xi Grants-in-Aid of Research.

REFERENCES

Anderson DE, Serences JT, Vogel EK, Awh E. Induced alpha rhythms track the content and quality of visual working memory representations with high temporal precision. Journal of Neuroscience. 2014; 34:7587–7599. [PubMed: 24872563]

Anderson JS. Origin of synchronized low-frequency blood oxygen level-dependent fluctuations in the primary visual cortex. AJNR. 2008; 29:1722–1729. [PubMed: 18635612]

Arnold M, Witte H, Leger P, Boccalon H, Bertuglia S, Colantuoni A. Time-variant spectral analysis of LDF signals on the basis of multivariate autoregressive modelling. Technology and Health Care. 1999; 7:103–112. [PubMed: 10463300]

Asada H, Fukuda Y, Tsunoda S, Yamaguchi M, Tonoike M. Frontal midline theta rhythms reflect alternative activation of prefrontal cortex and anterior cingulate cortex in humans. Neuroscience Letters. 1999; 274:29–32. [PubMed: 10530512]

Barak O, Tsodyks M, Romo R. Neuronal population coding of parametric working memory. Journal of Neuroscience. 2010; 30:9424–9430. [PubMed: 20631171]

Barttfeld P, Petroni A, Báez S, Urquina H, Sigman M, Cetkovich M, et al. Functional connectivity and temporal variability of brain connections in adults with attention deficit/hyperactivity disorder and bipolar disorder. Neuropsychobiology. 2014; 69:65–75. [PubMed: 24576926]

Bastiaansen M, Posthuma D, Groot PF, de Geus EJ. Event-related alpha and theta responses in a visuospatial working memory task. Clinical Neurophysiology. 2002; 113:1882–1893. [PubMed: 12464325]

Battaglia D, Brunel N, Hansel D. Temporal decorrelation of collective oscillations in neural networks with local inhibition and long-range excitation. Physical Review Letters. 2007; 99:238106. [PubMed: 18233419]

Bauer RH, Fuster JM. Delayed-matching and delayed-response deficit from cooling dorsolateral prefrontal cortex in monkeys. Journal of Comparative and Physiological Psychology. 1976; 90:293–302. [PubMed: 819472]

Bhowmik D, Shanahan M. Metastability and inter-band frequency modulation in networks of oscillating spiking neuron populations. PLoS One. 2013; 8:e62234. [PubMed: 23614040]

Bledowski C, Kaiser J, Rahm B. Basic operations in working memory: Contributions from functional imaging studies. Behavioural Brain Research. 2010; 214:172–179. [PubMed: 20678984]

Braver TS, Cohen JD, Nystrom LE, Jonides J, Smith EE, Noll DC. A parametric study of prefrontal cortex involvement in human working memory. Neuroimage. 1997; 5:49–62. [PubMed: 9038284]

Brovelli A, Ding M, Ledberg A, Chen Y, Nakamura R, Bressler SL. Beta oscillations in a large-scale sensorimotor cortical network: Directional influences revealed by Granger causality. Proceedings of the National Academy of Sciences, U.S.A. 2004; 101:9849–9854.

Buschman TJ, Denovellis EL, Diogo C, Bullock D, Miller EK. Synchronous oscillatory neural ensembles for rules in the prefrontal cortex. Neuron. 2012; 76:838–846. [PubMed: 23177967]

Buschman TJ, Miller EK. Top–down versus bottom–up control of attention in the prefrontal and posterior parietal cortices. Science. 2007; 315:1860–1862. [PubMed: 17395832]

Buzsaki G. Neural syntax: Cell assemblies, synapsembles, and readers. Neuron. 2010; 68:362–385. [PubMed: 21040841]

Buzsáki G, Draguhn A. Neuronal oscillations in cortical networks. Science. 2004; 304:1926–1929. [PubMed: 15218136]

Buzsáki G, Schomburg EW. What does gamma coherence tell us about inter-regional neural communication? Nature Neuroscience. 2015; 18:484–489. [PubMed: 25706474]

Canolty RT, Knight RT. The functional role of cross-frequency coupling. Trends in Cognitive Sciences. 2010; 14:506–515. [PubMed: 20932795]

Colby CL, Goldberg ME. Space and attention in parietal cortex. Annual Review of Neuroscience. 1999; 22:319–349.

Compte A, Brunel N, Goldman-Rakic PS, Wang XJ. Synaptic mechanisms and network dynamics underlying spatial working memory in a cortical network model. Cerebral Cortex. 2000; 10:910–923. [PubMed: 10982751]

Connolly JD, Goodale MA, Menon RS, Munoz DP. Human fMRI evidence for the neural correlates of preparatory set. Nature Neuroscience. 2002; 5:1345–1352. [PubMed: 12411958]

Courtney SM, Ungerleider LG, Keil K, Haxby JV. Object and spatial visual working memory activate separate neural systems in human cortex. Cerebral Cortex. 1996; 6:39–49. [PubMed: 8670637]

Critchley, M. The parietal lobes. Arnold; London: 1953.

Cui J, Xu L, Bressler SL, Ding M, Liang H. BSMART: A Matlab/C toolbox for analysis of multichannel neural time series. Neural Networks. 2008; 21:1094–1104. [PubMed: 18599267]

Curtis CE, D'Esposito M. Persistent activity in the prefrontal cortex during working memory. Trends in Cognitive Sciences. 2003a; 7:415–423. [PubMed: 12963473]

Curtis CE, D'Esposito M. Success and failure suppressing reflexive behavior. Journal of Cognitive Neuroscience. 2003b; 15:409–418. [PubMed: 12729492]

Damoiseaux JS, Rombouts SA, Barkhof F, Scheltens P, Stam CJ, Smith SM, et al. Consistent resting-state networks across healthy subjects. Proceedings of the National Academy of Sciences, U.S.A. 2006; 103:13848–13853.

D'Esposito M, Ballard D, Zarahn E, Aguirre GK. The role of prefrontal cortex in sensory memory and motor preparation: An event-related fMRI study. Neuroimage. 2000; 11:400–408. [PubMed: 10806027]

Ding M, Bressler SL, Yang W, Liang H. Short-window spectral analysis of cortical event-related potentials by adaptive multivariate autoregressive modeling: Data preprocessing, model validation, and variability assessment. Biological Cybernetics. 2000; 83:35–45. [PubMed: 10933236]

Doucet G, Naveau M, Petit L, Delcroix N, Zago L, Crivello F, et al. Brain activity at rest: A multiscale hierarchical functional organization. Journal of Neurophysiology. 2011; 105:2753–2763. [PubMed: 21430278]

Duff E, Johnston L, Xiong J, Fox P, Mareels I, Egan GF. The power of spectral density analysis for mapping endogenous BOLD signal fluctuations. Human Brain Mapping. 2008; 29:778–790. [PubMed: 18454458]

Eichele T, Debener S, Calhoun VD, Specht K, Engel AK, Hugdahl K, et al. Prediction of human errors by maladaptive changes in event-related brain networks. Proceedings of the National Academy of Sciences, U.S.A. 2008; 105:6173–6178.

Elton A, Gao W. Task related modulation of functional connectivity variability and its behavioral correlations. Human Brain Mapping. 2015; 36:3260–3272. [PubMed: 26015070]

Engel AK, Fries P, Singer W. Dynamic predictions: Oscillations and synchrony in top–down processing. Nature Reviews Neuroscience. 2001; 2:704–716. [PubMed: 11584308]

Fox MD, Snyder AZ, Vincent JL, Corbetta M, Van E, Raichle ME. The human brain is intrinsically organized into dynamic, anticorrelated functional networks. Proceedings of the National Academy of Sciences, U.S.A. 2005; 102:9673–9678.

Freeman WJ, Ahlfors SP, Menon V. Combining fMRI with EEG and MEG in order to relate patterns of brain activity to cognition. International Journal of Psychophysiology. 2009; 73:43–52. [PubMed: 19233235]

Freunberger R, Fellinger R, Sauseng P, Gruber W, Klimesch W. Dissociation between phase-locked and nonphase-locked alpha oscillations in a working memory task. Human Brain Mapping. 2009; 30:3417–3425. [PubMed: 19384888]

Fries P. A mechanism for cognitive dynamics: Neuronal communication through neuronal coherence. Trends in Cognitive Sciences. 2005; 9:474–480. [PubMed: 16150631]

Fries P, Reynolds JH, Rorie AE, Desimone R. Modulation of oscillatory neuronal synchronization by selective visual attention. Science. 2001; 291:1560–1563. [PubMed: 11222864]

Friston KJ. Another neural code? Neuroimage. 1997; 5:213–220. [PubMed: 9345550]

Funahashi S, Bruce CJ, Goldman-Rakic PS. Mnemonic coding of visual space in the monkey's dorsolateral prefrontal cortex. Journal of Neurophysiology. 1989; 61:331–349. [PubMed: 2918358]

Fuster JM. Unit activity in prefrontal cortex during delayed-response performance: Neuronal correlates of transient memory. Journal of Neurophysiology. 1973; 36:61–78. [PubMed: 4196203]

Fuster, JM. The prefrontal cortex. 4th. Academic Press; London: 2008.

Fuster JM. Cortex and memory: Emergence of a new paradigm. Journal of Cognitive Neuroscience. 2009; 21:2047–2072. [PubMed: 19485699]

Fuster JM, Bodner M, Kroger JK. Cross-modal and cross-temporal association in neurons of frontal cortex. Nature. 2000; 405:347–351. [PubMed: 10830963]

Fuster JM, Bressler SL. Cognit activation: A mechanism enabling temporal integration in working memory. Trends in Cognitive Sciences. 2012; 16:207–218. [PubMed: 22440831]

Fuster JM, Bressler SL. Past makes future: Role of pFC in prediction. Journal of Cognitive Neuroscience. 2015; 27:639–654. [PubMed: 25321486]

Gevins A, Smith ME, McEvoy L, Yu D. High-resolution EEG mapping of cortical activation related to working memory: Effects of task difficulty, type of precessing, and practice. Cerebral Cortex. 1997; 7:374–385. [PubMed: 9177767]

Haaland DM, Thomas EV. Partial least-squares methods for spectral analyses. 1. Relation to other quantitative calibration methods and the extraction of qualitative information. Analytical Chemistry. 1988; 60:1193–1202.

Hanslmayr S, Staudigl T, Fellner MC. Oscillatory power decreases and long-term memory: The information via desynchronization hypothesis. Frontiers in Human Neuroscience. 2012; 6:74. [PubMed: 22514527]

He BJ, Snyder AZ, Zempel JM, Smyth MD, Raichle ME. Electrophysiological correlates of the brain's intrinsic large-scale functional architecture. Proceedings of the National Academy of Sciences, U.S.A. 2008; 105:16039–16044.

Heilman, KM.; Pandya, DN.; Geschwind, N. Trimodal inattention following parietal lobe ablations. In: Trufant, SA., editor. Transactions of the American Neurological Association. Springer; New York: 1970. p. 259-261.

Honkanen R, Rouhinen S, Wang SH, Palva JM, Palva S. Gamma oscillations underlie the maintenance of feature-specific information and the contents of visual working memory. Cerebral Cortex. 2014; 25:3788–3801. [PubMed: 25405942]

Hutka S, Bidelman GM, Moreno S. Brain signal variability as a window into the bidirectionality between music and language processing: Moving from a linear to a nonlinear model. Frontiers in Psychology. 2013; 4:984. [PubMed: 24454295]

Ishii R, Shinosaki K, Ukai S, Inouye T, Ishihara T, Yoshimine T, et al. Medial prefrontal cortex generates frontal midline theta rhythm. NeuroReport. 1999; 10:675–679. [PubMed: 10208529]

Jensen O. Maintenance of multiple working memory items by temporal segmentation. Neuroscience. 2006; 139:237–249. [PubMed: 16337089]

Keijzer M, Jacques SL, Prahl SA, Welch AJ. Light distributions in artery tissue: Monte Carlo simulations for finite-diameter laser beams. Lasers in Surgery and Medicine. 1989; 9:148–154. [PubMed: 2716459]

Kiebel SJ, Tallon-Baudry C, Friston KJ. Parametric analysis of oscillatory activity as measured with EEG/ MEG. Human Brain Mapping. 2005; 26:170–177. [PubMed: 15929085]

Kilner J, Bott L, Posada A. Modulations in the degree of synchronization during ongoing oscillatory activity in the human brain. European Journal of Neuroscience. 2005; 21:2547–2554. [PubMed: 15932612]

Klimesch W. Memory processes, brain oscillations and EEG synchronization. International Journal of Psychophysiology. 1996; 24:61–100. [PubMed: 8978436]

Koch SP, Werner P, Steinbrink J, Fries P, Obrig H. Stimulus-induced and state-dependent sustained gamma activity is tightly coupled to the hemodynamic response in humans. Journal of Neuroscience. 2009; 29:13962–13970. [PubMed: 19890006]

Kohl M, Lindauer U, Royl G, Kuhl M, Gold L, Villringer A, et al. Physical model for the spectroscopic analysis of cortical intrinsic optical signals. Physics in Medicine & Biology. 2000; 45:3749–3764. [PubMed: 11131197]

Kostopoulos P, Albanese MC, Petrides M. Ventrolateral prefrontal cortex and tactile memory disambiguation in the human brain. Proceedings of the National Academy of Sciences, U.S.A. 2007; 104:10223–10228.

LaBar KS, Gitelman DR, Parrish TB, Mesulam M. Neuroanatomic overlap of working memory and spatial attention networks: A functional MRI comparison within subjects. Neuroimage. 1999; 10:695–704. [PubMed: 10600415]

Lachaux JP, Rodriguez E, Martinerie J, Varela FJ. Measuring phase synchrony in brain signals. Human Brain Mapping. 1999; 8:194–208. [PubMed: 10619414]

Leopold DA, Murayama Y, Logothetis NK. Very slow activity fluctuations in monkey visual cortex: Implications for functional brain imaging. Cerebral Cortex. 2003; 13:422–433. [PubMed: 12631571]

Lisman J. Working memory: The importance of theta and gamma oscillations. Current Biology. 2010; 20:R490–R492. [PubMed: 20541499]

Logothetis NK. What we can do and what we cannot do with fMRI. Nature. 2008; 453:869–878. [PubMed: 18548064]

Logothetis NK, Pauls J, Augath M, Trinath T, Oeltermann A. Neurophysiological investigation of the basis of the fMRI signal. Nature. 2001; 412:150–157. [PubMed: 11449264]

Lowet E, Roberts M, Hadjipapas A, Peter A, Eerden J, Weerd P. Input-dependent frequency modulation of cortical gamma oscillations shapes spatial synchronization and enables phase coding. PLOS Computational Biology. 2015; 11:e1004072. [PubMed: 25679780]

Mainardi LT. On the quantification of heart rate variability spectral parameters using time–frequency and time-varying methods. Philosophical Transactions of the Royal Society, Series A, Mathematical, Physical and Engineering Sciences. 2009; 367:255–275.

Mantini D, Perrucci MG, Del GC, Romani GL, Corbetta M. Electrophysiological signatures of resting state networks in the human brain. Proceedings of the National Academy of Sciences, U.S.A. 2007; 104:13170–13175.

Maris E, Oostenveld R. Nonparametric statistical testing of EEG- and MEG-data. Journal of Neuroscience Methods. 2007; 164:177–190. [PubMed: 17517438]

Matcher SJ, Elwell CE, Cooper CE, Cope M, Delpy DT. Performance comparison of several published tissue near-infrared spectroscopy algorithms. Analytical Biochemistry. 1995; 227:54–68. [PubMed: 7668392]

Mathiesen C, Caesar K, Lauritzen M. Temporal coupling between neuronal activity and blood flow in rat cerebellar cortex as indicated by field potential analysis. The Journal of Physiology. 2000; 523:235–246. [PubMed: 10673558]

Meltzer JA, Zaveri HP, Goncharova II, Distasio MM, Papademetris X, Spencer SS, et al. Effects of working memory load on oscillatory power in human intracranial EEG. Cerebral Cortex. 2008; 18:1843–1855. [PubMed: 18056698]

Mesulam M-M. A cortical network for directed attention and unilateral neglect. Annals of Neurology. 1981; 10:309–325. [PubMed: 7032417]

Meyers EM, Qi XL, Constantinidis C. Incorporation of new information into prefrontal cortical activity after learning working memory tasks. Proceedings of the National Academy of Sciences, U.S.A. 2012; 109:4651–4656.

Mitra, PP.; Bokil, H. Observed brain dynamics. Oxford University Press; New York: 2008.

Moosmann M, Ritter P, Krastel I, Brink A, Thees S, Blankenburg F, et al. Correlates of alpha rhythm in functional magnetic resonance imaging and near infrared spectroscopy. Neuroimage. 2003; 20:145–158. [PubMed: 14527577]

Obrig H, Villringer A. Beyond the visible—Imaging the human brain with light. Journal of Cerebral Blood Flow & Metabolism. 2003; 23:1–18.

Palva S, Kulashekhar S, Hämäläinen M, Palva JM. Localization of cortical phase and amplitude dynamics during visual working memory encoding and retention. Journal of Neuroscience. 2011; 31:5013–5025. [PubMed: 21451039]

Pesaran B, Pezaris JS, Sahani M, Mitra PP, Andersen RA. Temporal structure in neuronal activity during working memory in macaque parietal cortex. Nature Neuroscience. 2002; 5:805–811. [PubMed: 12134152]

Pessoa L, Gutierrez E, Bandettini P, Ungerleider L. Neural correlates of visual working memory: fMRI amplitude predicts task performance. Neuron. 2002; 35:975–987. [PubMed: 12372290]

Quintana J, Fuster JM. From perception to action: Temporal integrative functions of prefrontal and parietal neurons. Cerebral Cortex. 1999; 9:213–221. [PubMed: 10355901]

Rack-Gomer AL, Liu TT. Caffeine increases the temporal variability of resting-state BOLD connectivity in the motor cortex. Neuroimage. 2012; 59:2994–3002. [PubMed: 22032947]

Raichle ME. The restless brain: How intrinsic activity organizes brain function. Philosophical Transactions of the Royal Society of London, Series B, Biological Sciences. 2015; 370:1–11.

Raichle ME, Mintun MA. Brain work and brain imaging. Annual Review of Neuroscience. 2006; 29:449–476.

Ray S, Maunsell JH. Do gamma oscillations play a role in cerebral cortex? Trends in Cognitive Sciences. 2015; 19:78–85. [PubMed: 25555444]

Ricciardi E, Bonino D, Gentili C, Sani L, Pietrini P, Vecchi T. Neural correlates of spatial working memory in humans: A functional magnetic resonance imaging study comparing visual and tactile processes. Neuroscience. 2006; 139:339–349. [PubMed: 16324793]

Rizzuto DS, Madsen JR, Bromfield EB, Schulze-Bonhage A, Seelig D, Schenbrenner-Scheibe R, et al. Reset of human neocortical oscillations during a working memory task. Proceedings of the National Academy of Sciences, U.S.A. 2003; 100:7931–7936.

Romo R, Brody CD, Hernández A, Lemus L. Neuronal correlates of parametric working memory in the prefrontal cortex. Nature. 1999; 399:470–473. [PubMed: 10365959]

Roux F, Wibral M, Mohr HM, Singer W, Uhlhaas PJ. Gamma-band activity in human prefrontal cortex codes for the number of relevant items maintained in working memory. Journal of Neuroscience. 2012; 32:12411–12420. [PubMed: 22956832]

Sadaghiani S, Scheeringa R, Lehongre K, Morillon B, Giraud AL, D'Esposito M, et al. Alpha-band phase synchrony is related to activity in the fronto-parietal adaptive control network. Journal of Neuroscience. 2012; 32:14305–14310. [PubMed: 23055501]

Salazar RF, Dotson NM, Bressler SL, Gray CM. Content-specific fronto-parietal synchronization during visual working memory. Science. 2012; 338:1097–1100. [PubMed: 23118014]

Sarnthein J, Petsche H, Rappelsberger P, Shaw GL, von Stein A. Synchronization between prefrontal and posterior association cortex during human working memory. Proceedings of the National Academy of Sciences, U.S.A. 1998; 95:7092–7096.

Sauseng P, Klimesch W, Heise KF, Gruber WR, Holz E, Karim AA, et al. Brain oscillatory substrates of visual short-term memory capacity. Current Biology. 2009; 19:1846–1852. [PubMed: 19913428]

Scholvinck ML, Maier A, Ye FQ, Duyn JH, Leopold DA. Neural basis of global resting-state fMRI activity. Proceedings of the National Academy of Sciences, U.S.A. 2010; 107:10238–10243.

Shindy WW, Posley KA, Fuster JM. Reversible deficit in haptic delay tasks from cooling prefrontal cortex. Cerebral Cortex. 1994; 4:443–450. [PubMed: 7950314]

Shmuel A, Leopold DA. Neuronal correlates of spontaneous fluctuations in fMRI signals in monkey visual cortex: Implications for functional connectivity at rest. Human Brain Mapping. 2008; 29:751–761. [PubMed: 18465799]

Siegel M, Donner TH, Engel AK. Spectral fingerprints of large-scale neuronal interactions. Nature Reviews Neuroscience. 2012; 13:121–134. [PubMed: 22233726]

Siegel M, Warden MR, Miller EK. Phase-dependent neuronal coding of objects in short-term memory. Proceedings of the National Academy of Sciences, U.S.A. 2009; 106:21341–21346.

Smith SM, Miller KL, Moeller S, Xu J, Auerbach EJ, Woolrich MW, et al. Temporally-independent functional modes of spontaneous brain activity. Proceedings of the National Academy of Sciences, U.S.A. 2012; 109:3131–3136.

Snyder LH, Batista AP, Andersen RA. Coding of intention in the posterior parietal cortex. Nature. 1997; 386:167–170. [PubMed: 9062187]

Sreenivasan K, Curtis C, D'Esposito M. Revisiting the role of persistent neural activity during working memory. Trends in Cognitive Sciences. 2014; 18:82–89. [PubMed: 24439529]

Steinbrink J, Villringer A, Kempf F, Haux D, Boden S, Obrig H. Illuminating the BOLD signal: Combined fMRI-fNIRS studies. Magnetic Resonance Imaging. 2006; 24:495–505. [PubMed: 16677956]

Stokes MG, Kusunoki M, Sigala N, Nili H, Gaffan D, Duncan J. Dynamic coding for cognitive control in prefrontal cortex. Neuron. 2013; 78:364–375. [PubMed: 23562541]

Stokić M, Milovanović D, Ljubisavljević MR, Nenadović V, Čukić M. Memory load effect in auditory–verbal short-term memory task: EEG fractal and spectral analysis. Experimental Brain Research. 2015; 233:1–16. [PubMed: 25248844]

Sylvester CM, Shulman GL, Jack AI, Corbetta M. Anticipatory and stimulus-evoked blood oxygenation level-dependent modulations related to spatial attention reflect a common additive signal. Journal of Neuroscience. 2009; 29:10671–10682. [PubMed: 19710319]

Tallon-Baudry C, Bertrand O, Fischer C. Oscillatory synchrony between human extrastriate areas during visual short-term memory maintenance. Journal of Neuroscience. 2001; 21:RC177. [PubMed: 11588207]

Tallon-Baudry C, Kreiter A, Bertrand O. Sustained and transient oscillatory responses in the gamma and beta bands in a visual short-term memory task in humans. Visual Neuroscience. 1999; 16:449–459. [PubMed: 10349966]

Uludag K, Kohl M, Steinbrink J, Obrig H, Villringer A. Cross talk in the Lambert-Beer calculation for near-infrared wavelengths estimated by Monte Carlo simulations. Journal of Biomedical Optics. 2002; 7:51–59. [PubMed: 11818012]

Vaadia E, Benson DA, Hienz RD, Goldstein MH. Unit study of monkey frontal cortex: Active localization of auditory and of visual stimuli. Journal of Neurophysiology. 1986; 56:934–952. [PubMed: 3783237]

Vanzetta I, Grinvald A. Coupling between neuronal activity and microcirculation: Implications for functional brain imaging. Human Frontier Science Program Journal. 2008; 2:79–98.

Villringer A, Chance B. Non-invasive optical spectroscopy and imaging of human brain function. Trends in Neurosciences. 1997; 20:435–442. [PubMed: 9347608]

Vincent JL, Patel GH, Fox MD, Snyder AZ, Baker JT, Van E, et al. Intrinsic functional architecture in the anaesthetized monkey brain. Nature. 2007; 447:83–86. [PubMed: 17476267]

Wang XJ. Neurophysiological and computational principles of cortical rhythms in cognition. Physiological Reviews. 2010; 90:1195–1268. [PubMed: 20664082]

Womelsdorf T, Fries P. The role of neuronal synchronization in selective attention. Current Opinion in Neurobiology. 2007; 17:154–160. [PubMed: 17306527]

Womelsdorf T, Schoffelen JM, Oostenveld R, Singer W, Desimone R, Engel AK, et al. Modulation of neuronal interactions through neuronal synchronization. Science. 2007; 316:1609–1612. [PubMed: 17569862]

Wray S, Cope M, Delpy DT, Wyatt JS, Reynolds EO. Characterization of the near infrared absorption spectra of cytochrome aa3 and haemoglobin for the non-invasive monitoring of cerebral oxygenation. Biochimica et Biophysica Acta. 1988; 933:184–192. [PubMed: 2831976]

Yeo BT, Krienen FM, Sepulcre J, Sabuncu MR, Lashkari D, Hollinshead M, et al. The organization of the human cerebral cortex estimated by intrinsic functional connectivity. Journal of Neurophysiology. 2011; 106:1125–1165. [PubMed: 21653723]

Zhou YD, Ardestani A, Fuster JM. Distributed and associative working memory. Cerebral Cortex. 2007; 17(Suppl. 1):i77–i87. [PubMed: 17615249]

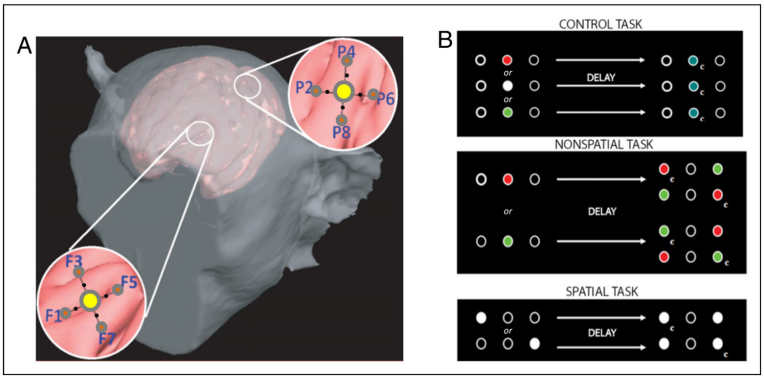

Figure 1.

Experimental paradigm. (A) ROIs and recording probe orientation. Circles on the cortical surface reconstruction indicate the positions of the epidural surgical implants. The call-out circles show a magnified view of each ROI. To ensure accurate resampling over successive sessions, two perpendicular axes (fine lines) are defined across each ROI, with which the recording probes are aligned. Recording channels designated as F1–F7 and P2–P8 refer to sampling positions in pFC and PPC, respectively. Yellow circle, light emitter; orange circle, detector; black dot, electrode. (B) Behavioral tasks. The task panel contains a horizontal array of three touch responsive display buttons that register the animal's manual selections by photocells. Each row in the diagram depicts the possible stimulus presentation sequences in each of the respective tasks. c = correct choice.

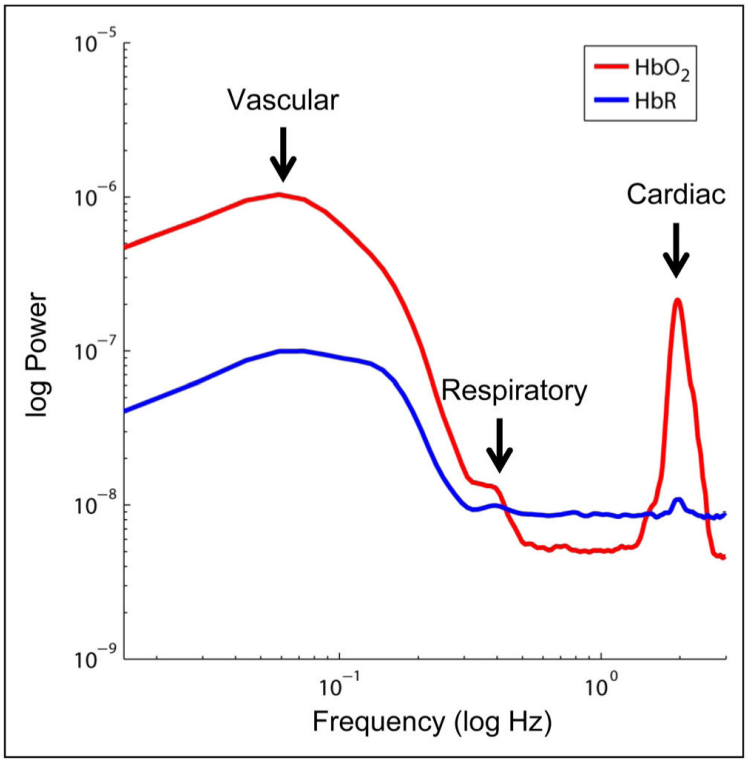

Figure 2.

NIRS power spectrum at rest. Mean power spectra across all subjects show spectral inflections at approximately 0.08, 0.3, and 1.9 Hz in both the HbO_2 and HbR signals. These peaks correspond to vascular, respiratory, and cardiac rhythms, respectively. Nonvascular (i.e., artifactual) signal constitutes a greater relative proportion of total power in the HbO_2 signal than in the HbR signal.

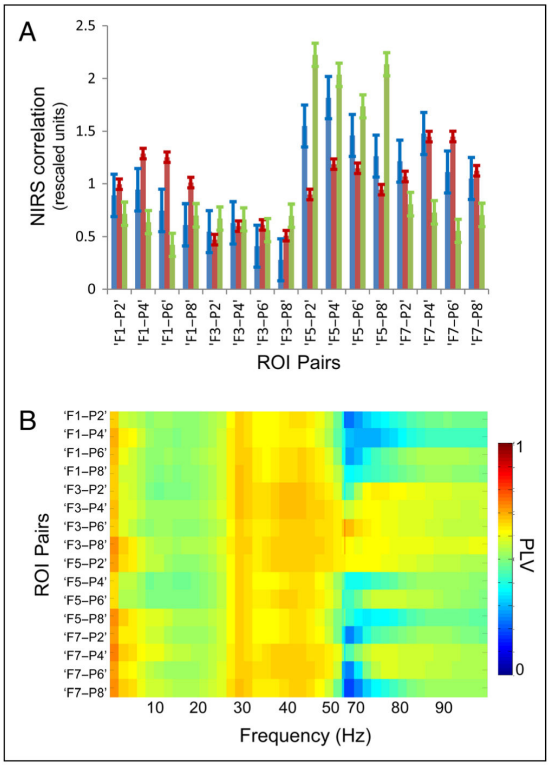

Figure 3.

Interregional resting state signal interactions. (A) Histograms of average pairwise NIRS correlation values at rest are plotted for three subjects. Values for each interregional ROI pair are plotted along the abscissa. Error bars represent the standard error. (B) Grand-averaged interregional SFP PLVs across all subjects. Values between 55 and 65 Hz were contaminated by powerline artifact and are excluded for clarity. Color bar denotes absolute PLV.

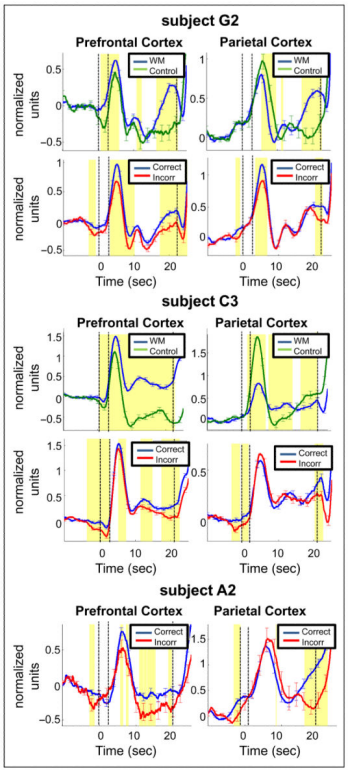

Figure 4.

NIRS amplitude during task performance. Each plot is standardized with respect to its own baseline. For subjects G2 and C3, the top pair of panels depicts the mean NIRS time course for WM and control task trials, whereas the lower pair does the same for correct and incorrect performance. Highlighted segments indicate significant difference between the two conditions ($p < .05$ on a cluster permutation distribution from 5000 iterations). Error bars denote variance computed across trials. Vertical dotted lines demarcate the stimulus (cue) epoch at $t = 0–2$ sec, and the choice stimulus at $t = 22$ sec. Control task data were not recorded from subject A2.

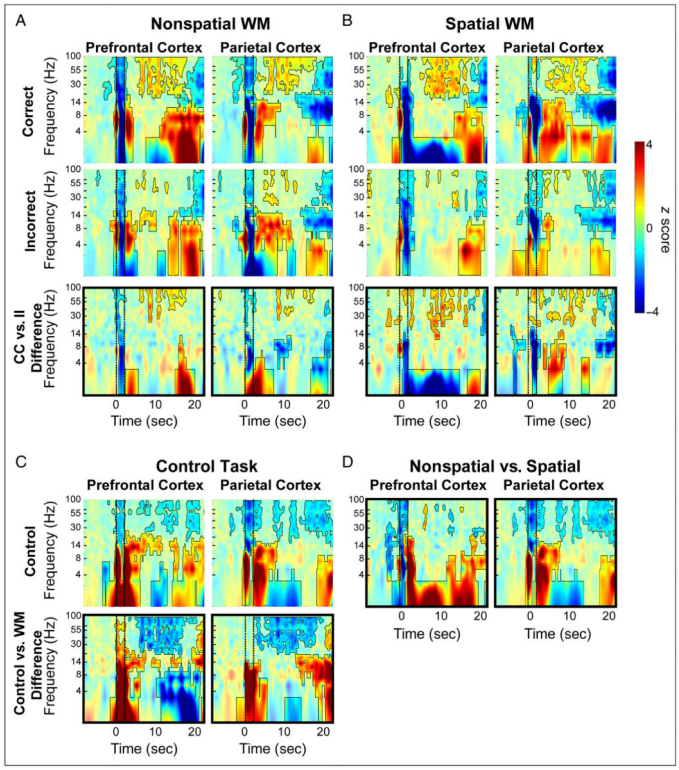

Figure 5.

TFRs of SFP band-power during task performance for subject G2. (A) Nonspatial WM task. TFRs are separately shown for correct (top row) and incorrect (second row) trials, in both prefrontal and parietal regions. The third row of TFR maps, delineated by a black outline, depicts the difference map between the two conditions. The color scale denotes *z* scores of oscillatory power changes with respect to baseline. Heavily colored, outlined regions of the maps indicate time–frequency clusters that significantly differ from baseline ($p < .001$, cluster permutation distribution, 5000 iterations). (B) Nonspatial WM task and (C) Control task. Conventions are the same as those described in (A). (D) Memorandum-dependent differences in SFP band-power. TFR difference maps between WM trials of nonspatial and spatial memoranda.

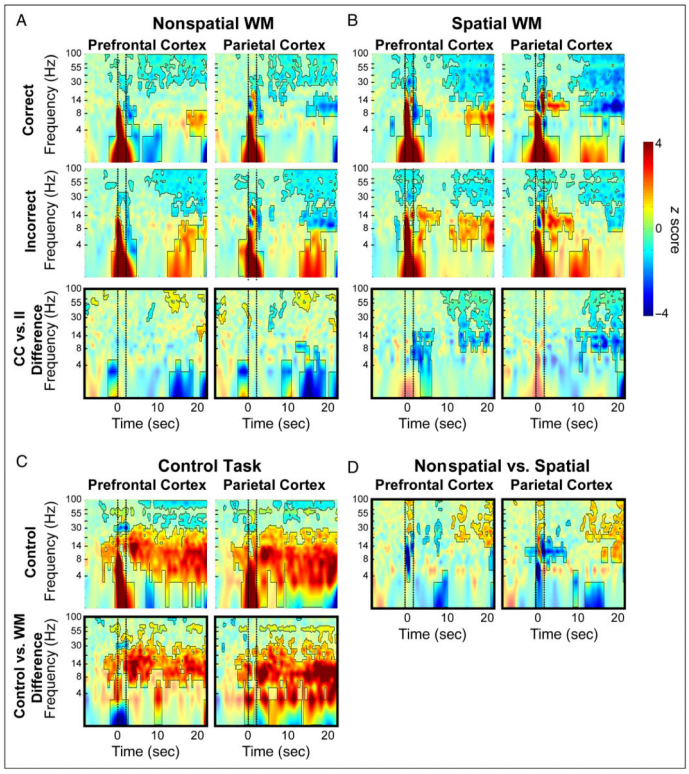

Figure 6.

TFRs of SFP band-power during task performance for subject C3. Conventions are the same as those described in Figure 5.

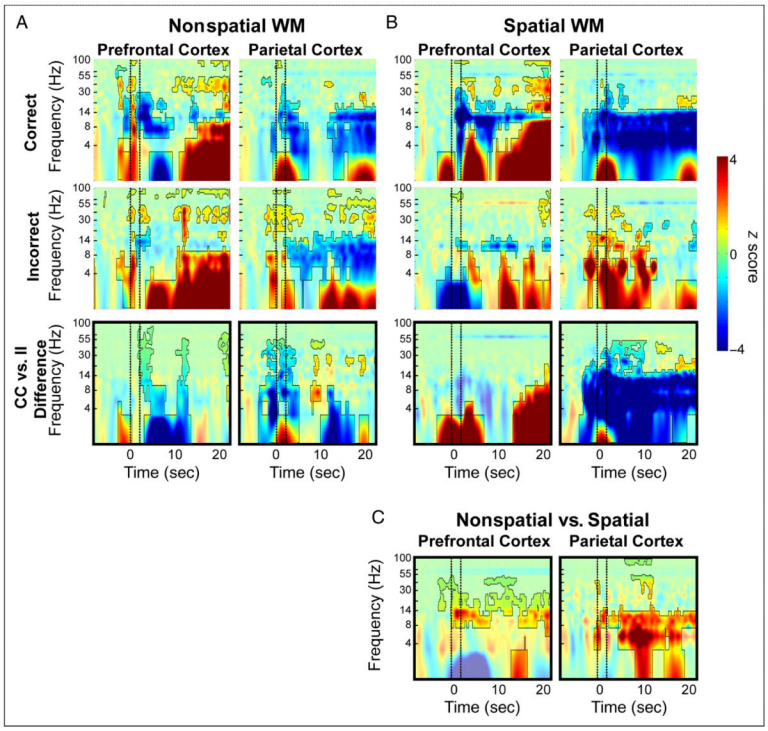

Figure 7.

TFRs of SFP band-power during task performance for subject A2. Conventions are the same as those described in Figure 5. The WM delay epoch in this subject exhibits a sustained, performance-dependent desynchronization in lower frequencies. Although this signal feature differs from band-power trends seen in the other subjects, it accords well with WM dynamics reported elsewhere (Bastiaansen, Posthuma, Groot, & de Geus, 2002; Tallon-Baudry et al., 1999). subject A2 did not undergo data collection during performance of the control task.

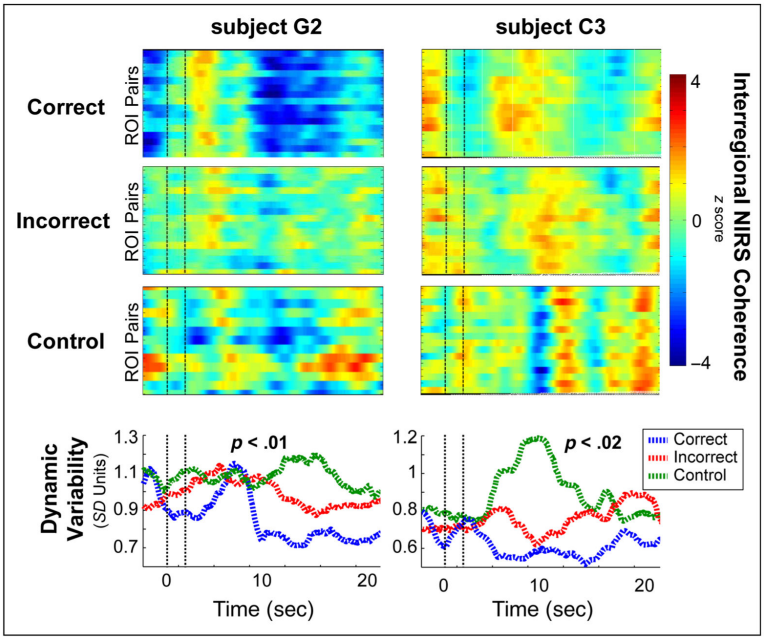

Figure 8.

Interregional NIRS coactivations during task performance. (A) Mean interregional NIRS coherence values were computed for correct, incorrect, and control task trials using MVAR modeling and standardized with respect to baseline. Each coherence map contains 16 rows of data, each corresponding to the mean fluctuations of NIRS coherence (in *z* scores) of an interregional ROI pair. Vertical dotted lines indicate the stimulus presentation epoch. Correct trials characteristically show a robust, uniform increase in interregional coherence followed by an equally well-demarcated relative decrease in coherence. That pattern is attenuated in incorrect and control task trials. (B) Variability of interregional coherence across trial epochs. A sliding computation of variance was performed using a 5-sec window, translated in 1-sec overlapping increments, applied across all frontoparietal ROI pairs. The plots therefore represent the combined variability in time and space (across interregional signal pairs). The delay period in both subjects shows significant task-dependent differences in uniformity of interregional coherence throughout the entire delay epoch (Kruskal–Wallis test; $p = .01$ for subject G2, $p = .02$ for subject C3), but none in the baseline period. Maximal variability is present in control task trials, and relatively constant variability is present in correct trials. The effect is most prominent during the late delay in subject G2 and in the early delay in subject C3.

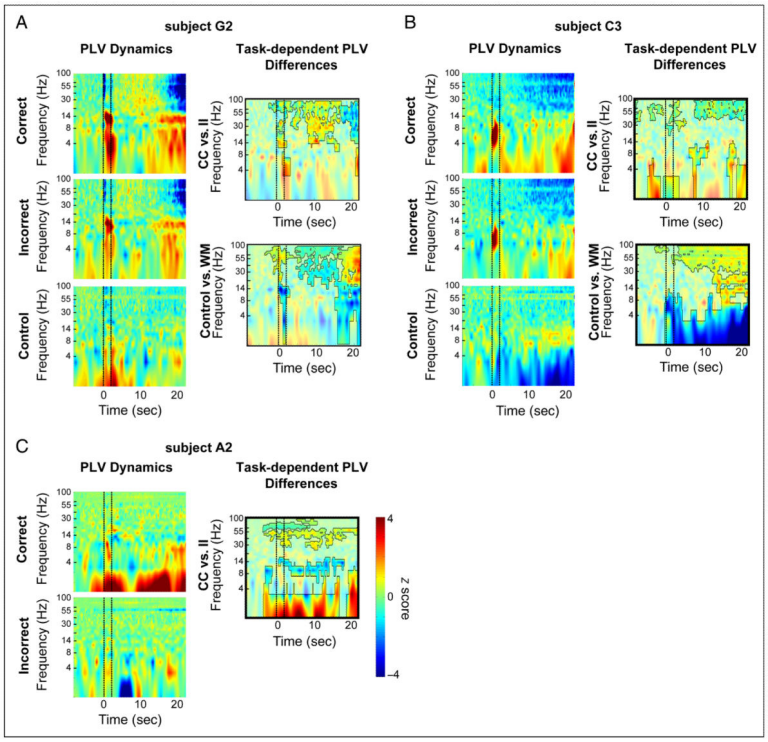

Figure 9.

Interregional SFP phase-locking during task performance for subject G2 (A), subject C3 (B), and subject A2 (C). Left: TFR maps show interregional phase-locking dynamics separately for correct, incorrect, and control task trials. The color scale denotes *z* scores of oscillatory power changes with respect to baseline. Right: TFR difference maps depict differences in phase-locking between correct and incorrect trials (CC vs. II) and between control task and WM trials (control vs. WM). In all maps, the color scale denotes *z* scores of oscillatory power changes with respect to baseline. Heavily colored, outlined regions of the maps indicate time–frequency clusters that significantly differ from baseline ($p < .001$, cluster permutation distribution, 5000 iterations).

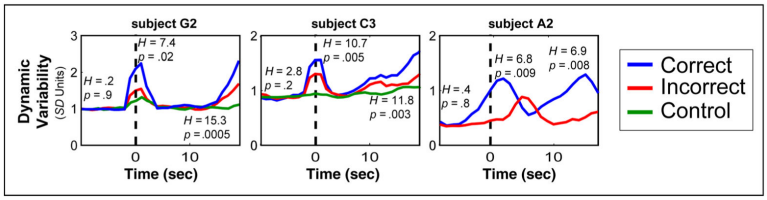

Figure 10.

Variability of interregional SFP phase-locking across trial epochs. A sliding computation of variance was performed using a 3-sec window, translated in 1-sec overlapping increments, across all analyzed frequencies (1–100 Hz). For each subject, plots of dynamic variability are computed for correct (blue), incorrect (red), and control task (green) trials. The results of the Kruskal–Wallis *H*-statistic and corresponding *p* value are depicted separately for the baseline ($t = -11$ to -5 sec), peristimulus ($t = -1$ to 5 sec), and late-delay ($t = 16$–22 sec) epochs.

Table 1

Total Database of Signals Acquired in the Resting State and during WM Task Performance

	NIRS		*SFP*	
Subject	***Resting State (min)***	***WM (No. of Trials)***	***Resting State (min)***	***WM (No. of Trials)***
G2	230	1948	230	1478
C3	193	2641	193	2129
A2	129	1414	129	1028

The size of the respective databases is described in terms of acquisition time (in minutes) for the resting state and in trial number for WM task performance. Only resting state epochs and WM trials in which both signal modes met screening criteria (see Methods) were included in the analysis. Two subjects (C3 and G2) underwent NIRS-SFP recording while performing the WM and control tasks, whereas subject A2 provided only NIRS-SFP recordings during WM performance. In the WM tasks, the subjects' correct response rates ranged from 77% to 81%.

Table 2

Variability of Interregional SFP Phase-locking in Different Band-limited Components

	Baseline			*Cue/Early Delay (−2 to 3 sec)*			*Late Delay (17–22 sec)*		
	subject G2	***subject C3***	***subject A2***	***subject G2***	***subject C3***	***subject A2***	***subject G2***	***subject C3***	***subject A2***
High gamma (65–100 Hz)	$H = 2.0$	$H = 1.9$	$U = 3.6$	$H = 11.6$	$H = 6.4$	$U = 3.9$	$H = 10.8$	$H = 13.9$	$U = 3.6$
	$p = .4$	$p = .4$	$p = .06$	$p = .003$	$p = .04$	$p = .048$	$p = .004$	$p = .001$	$p = .06$
Gamma (41–55 Hz)	$H = 2.2$	$H = 5.9$	$U = 0.9$	$H = 8.1$	$H = 6.9$	$U = 14.8$	$H = 16.8$	$H = 10.2$	$U = 4.2$*
	$p = .3$	$p = .052$	$p = .3$	$p = .02$	$p = .03$	$p = .001$	$p = .0002$	$p = .006$	$p = .04$
Low gamma (31–40 Hz)	$H = 2.4$	$H = 1.7$	$U = 7.0$	$H = 10.6$	$H = 0.9$	$U = 7.0$	$H = 7.6$	$H = 0.6$	$U = 8.4$
	$p = .3$	$p = .4$	$p = .01$	$p = .004$	$p = .6$	$p = .01$	$p = .02$	$p = .7$	$p = .004$
Beta (21–30 Hz)	$H = 3.8$	$H = 1.6$	$U = 3.7$	$H = 1.3$	$H = 0.5$	$U = 10.2$	$H = 8.0$	$H = 2.0$	$U = 1.1$
	$p = .15$	$p = .4$	$p = .054$	$p = .5$	$p = .8$	$p = .001$	$p = .02$	$p = .4$	$p = .3$
Low beta (15–20 Hz)	$H = 5.7$	$H = 0.9$	$U = 0.6$	$H = 3.1$	$H = 12.8$*	$U = 8.2$	$H = 12.5$	$H = 9.2$	$U = 9.9$
	$p = .06$	$p = .6$	$p = .4$	$p = .2$	$p = .002$	$p = .004$	$p = .002$	$p = .01$	$p = .002$
Alpha (9–14 Hz)	$H = 0.6$	$H = 3.0$	$U = 0.5$	$H = 6.9$	$H = 6.4$	$U = 14.5$	$H = 5.8$	$H = 3.6$	$U = 4.8$
	$p = .7$	$p = .2$	$p = .5$	$p = .03$	$p = .04$	$p = .0001$	$p = .06$	$p = .2$	$p = .03$
Theta (5–8 Hz)	$H = 2.0$	$H = 0.3$	$U = 1.0$	$H = 4.5$	$H = 8.0$	$U = 0.4$	$H = 2.9$	$H = 6$*	$U = 5.3$*
	$p = .4$	$p = .8$	$p = .3$	$p = .1$	$p = .02$	$p = .5$	$p = .2$	$p = .05$	$p = .02$
Delta (1–4 Hz)	$H = 0.7$	$H = 1.5$	$U = 5.5$	$H = 1.4$	$H = 5.0$	$U = 0.3$	$H = 5.7$	$H = 1.2$	$U = 6.9$
	$p = .7$	$p = .4$	$p = .02$	$p = .5$	$p = .08$	$p = .6$	$p = .06$	$p = .55$	$p = .01$

This table depicts the task-dependent differences illustrated in Figure 10 as a function of the constituent frequency bands. For each subject, trial epoch, and frequency band, a Kruskal–Wallis test was used to compare differences in dynamic variability between correct WM, incorrect WM, and control task trials. For each comparison, an H statistic and a p value are noted. Entries in red font correspond to statistically significant conditions in which correct WM trials show the greatest dynamic variability and control task trials the least. Asterisks denote significant deviations from that order of differentiation of variability.